NUMERICAL SIMULATION OF VORTEX-INDUCED VIBRATIONS OF RISER-CONDUCTOR SYSTEMS INCLUDING SOIL-STRUCTURE INTERACTIONS

A Thesis

by

MAOKUN YE

Submitted to the Office of Graduate and Professional Studies of
Texas A&M University
in partial fulfillment of the requirements for the degree of

MASTER OF SCIENCE

Chair of Committee,	Hamn-Ching Chen
Committee Members,	Scott Socolofsky
	James Kaihatu
Head of Department,	Sharath Girimaji

August 2018

Major Subject: Ocean Engineering

ABSTRACT

A fully three-dimensional numerical approach for analyzing deepwater drilling riser-conductor system vortex-induced vibrations (VIV) including soil-structure interactions (SSI) is presented. The drilling riser-conductor system is modeled as a tensioned beam with linearly distributed tension and is solved by a fully implicit discretization scheme. The fluid field around the riser-conductor system is obtained by Finite-Analytic Navier-Stokes (FANS) code, which numerically solves the unsteady Navier-Stokes equations. The SSI is taken into account by modeling the lateral soil resistance force according to p-y curves. Overset grid method is adopted to mesh the fluid domain with approximately 0.86 million computational points in total. Meshes are much finer in regions close to the pipe outer boundary and coarser in the far-field regions. A partitioned Fluid-Structure Interaction (FSI) method is achieved by communication between the fluid solver and pipe motion solver.

A pipe VIV simulation without SSI is firstly presented and served as a benchmark case for following simulations. Two SSI models based on a popular p-y curve are then applied to the VIV simulations. Results from those simulations are compared and analyzed. The effects of two key soil properties on the VIV simulations of riser-conductor systems are then studied. Conclusions are made and suggestions are given for VIV analysis of riser-conductor systems and future research.

DEDICATION

This thesis is dedicated to my wife, Wan Huang, who has been a Ph.D. student in Department of Sociology in TAMU this year. My wife and I were classmates in high school and we were in two distant cities and even two countries for five years, and we got married in summer 2017. Thanks to the perseverance we both have showed. And thanks for always being a constant source of support and encouragement during my graduate school studies.

This thesis is also dedicated to my parents, Zhongbin Ye and Xiangjun Liu. Thanks for their steadfast support both financially and mentally, without whom none of this work is possible.

Last, this thesis is also dedicated to my grandparents, who are always bringing me peace.

ACKNOWLEDGEMENTS

I would like to sincerely thank my committee chair, Dr. Chen, and my committee members, Dr. Socolofsky and Dr. Kaihatu, for their guidance and support throughout the course of this research.

Thanks also go to my friends and classmates and the department faculty and staff for making my time at Texas A&M University a great experience. Finally, thanks to my father and mother and my wife for their encouragement and support.

Last but not the least, I want to thank the Texas A&M University High Performance Research Computing Center for the necessary computer resources provided, which enabled me to work efficiently.

CONTRIBUTORS AND FUNDING SOURCES

This thesis was supervised by a thesis committee consisting of Dr. Hamn-Ching Chen, Dr. Scott Socolofsky and Dr. James Kaihatu of the Department of Ocean Engineering and the Department of Civil Engineering.

All work for the thesis was completed independently by the student.

There are no outside funding contributions to acknowledge related to this research.

NOMENCLATURE

CFD	Computational Fluid Dynamic
VIV	Vortex-Induced Vibration
FSI	Fluid-Structure Interaction
SSI	Soil-Structure Interaction
p-y	Load-Deflection
LES	Large Eddy Simulation
RANS	Reynolds-Averaged Navier-Stokes
FANS	Finite-Analytic Navier-Stokes

TABLE OF CONTENTS

LIST OF FIGURES

LIST OF TABLES

1. INTRODUCTION AND LITERATURE REVIEW

1.1. Overview

Offshore oil production (including lease condensate and hydrocarbon gas liquids) has experienced a continual increase globally during last few decades and accounted for about 30% of total oil production over the past decade.

In particular, as shown in Figure 1, deepwater (water depth greater than 125 meters) production, or in some areas, ultra-deepwater (at water depths of 1,500 meters or more) production has become more and more important, due to changing economics and the exhaustion of shallow offshore resources.

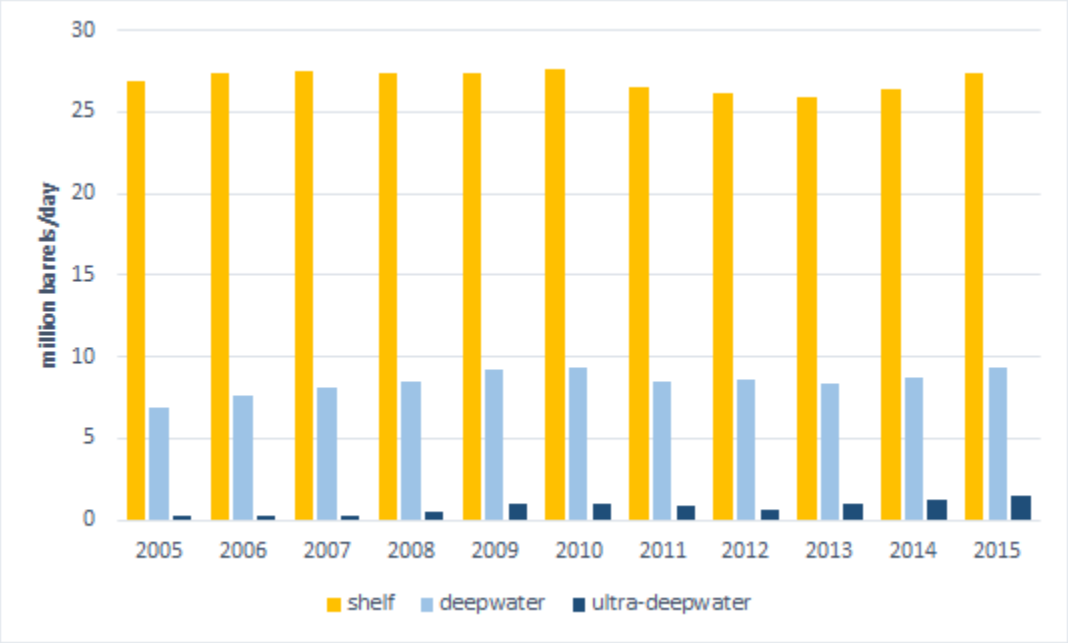

Figure 1 Global Offshore Production by Water Depth

However, due to the complex and harsh loads in the ocean environment (wind, currents, wave actions, and ship impacts), the deepwater production is characterized by high-cost and high-risk. In deepwater production operations, stable and reliable subsea wellhead and drilling system are of great importance. Therefore, research on the responses of those structures under environmental loads is of great importance.

This thesis will contribute additional knowledge to analysis and design methods for offshore riser-conductor systems, by a set of simulations using numerical methods. And this thesis will help to improve general understandings of the behavior of deepwater riser-conductor systems under vortex-induced vibrations.

1.2. Offshore Pipelines and Drilling Conductors

Pipelines are widely used in offshore oil production industry. Many offshore structures can be modeled as top-tensioned or catenary pipes, including drilling risers, platform legs, conductors etc. Pipelines are typical slender structures, with length up to several hundred meters and cross-section diameter less than two meters.

Offshore oil production conductors are the widest diameter pipes (Ilupeju, 2014). They are used for offshore wells and serve as a foundation for the wellhead, as shown in Figure 2. They are surrounded by seabed soil and usually connected to floating moored production platforms through a top-tensioned riser.

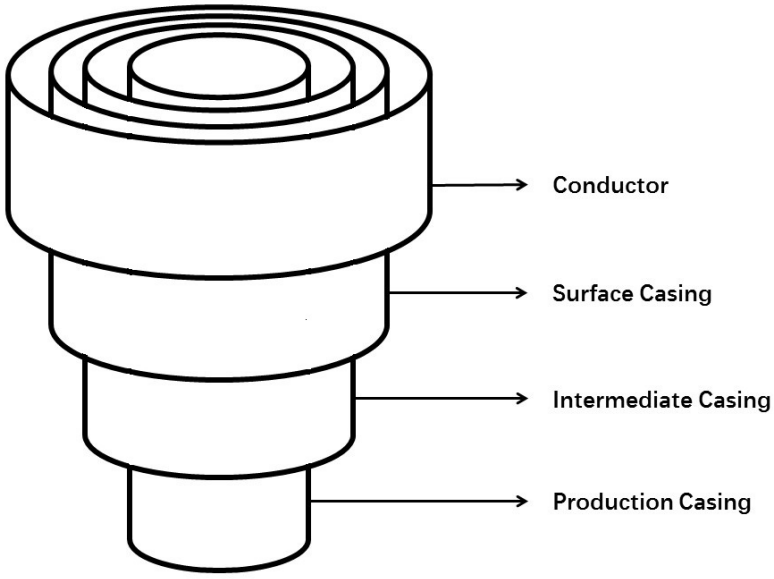

Figure 2 Conductor

The extremely complex loads experienced by the riser-conductor system, including ocean currents and waves, platform motions and soil resistance force, can potentially cause damages to the system. Especially when the system is experiencing vortex induced vibrations, significant cyclic fluid loads can occur, which results to a considerable reduction in system reliability and fatigue life.

1.3. Vortex Induced Vibrations of Offshore Pipelines

Riser Vortex induced Vibration (VIV) has been studied by many researchers and has been an active research area in Ocean Engineering for several years, and both experimental studies and numerical simulations have been applied to this research area.

During the last few decades, VIV experiments were carried out by many researchers and institutions. Wilde and Huijsmans (2004) from Maritime Research Institute Netherlands (MARIN), conducted a laboratory experiment, in which a steel pipe with circular cross section was studied. The diameter and length of the pipe were 16mm and 12.6m respectively. Pipe VIV behaviors from several towing speeds (0.5 to 3.0 m/s) and pretentions (0.5 to 2.5 kN) were recorded. Trim et al. (2005) conducted a test in Marintek's Ocean Basin of a pipe model with a length-to-diameter ratio equal to 1400, in an effort to more accurately predict the fatigue life of risers. Some key considerations and suggested design methods are presented according to the experiment. Full-scale riser VIV responses are collected in Gulf of Mexico and reported by Tognarelli et al. (2008), and the data is compared with the VIV results obtained from commercial software.

With the development of computer capability and computational methods, numerical simulations to study pipeline VIV are widely used. Simulations of VIV response for fixed cylinders are conducted by Pontaza, Chen and Chen (2004), by using a Computational Fluid Dynamics (CFD) method combined with overset grid technique. Following studies on long risers with length-to-diameter ratio of 1400 were carried out by Huang, Chen and Chen (2007). A simplified pipe motion solver with only in-line and cross-flow displacement was proposed and validated. Same methods were further applied to the simulations of VIV and Wake-Induced Vibrations (WIV) of dual Risers by Chen, Chen and Huang (2013). A beam finite element coupled with a viscous flow

solver was used to simulate the VIV of pipes by Pontaza and Menon (2009), and a good agreement with previous research and experiment were reported.

1.4. Soil-Structure Interactions (SSI)

1.4.1. Background

Risers are typically pinned at both ends in previous research and the only load applied to the pipe is the fluid force. However, this might not be true for offshore riser-conductor systems in real ocean environment. Offshore drilling conductors penetrate into seabed in real cases, thus soil resistance forces will be unavoidably applied to riser-conductor systems. And for the reason that the riser-conductor systems are not pinned at mudline, lateral displacement in both in-line and cross-flow directions will occur within the seabed soil. In other words, SSI should be taken into account in riser-conductor system VIV simulations.

1.4.2. Response of Piles Under Lateral loadings

1.4.2.1. Beam on Winkler Foundation Method

Offshore riser-conductor systems with SSI considered can be modeled as so called ' laterally loaded piles' in soil. In past several decades, the behavior of ' laterally loaded piles' in soil has been studied by many researchers, and several popular SSI analysis methods were proposed. Including Beam on Winkler Foundation method (Nogami et al., 1988,1991; Gazetas and Dorbry, 1984; Naggar and Novak, 1995) continuous medium model method (Basu and Salgado, 2007; Han, Salgado and Prezzi, 2015), and experimental method (Reese, 1974). In particular, due to its obvious physical

meaning and less computational effort, Beam on Winkler Foundation method has been widely used in numerical simulations of pile-soil interactions.

Beam on Winkler Foundation method is an approach to treat continual soil resistance force as discretized equivalent soil springs. Many soil models have been published for last several decades.

Novak et al. (1974) modeled the soil resistance force as a series of frequency dependent springs and dashpots. An approximate analytical approach based on linear elasticity is introduced in the work, but only simple harmonic excitation with linear soil properties could be analyzed by this method. A relatively complicated method to model the soil resistance as near field and far field springs is presented by Nogami et al. (1988). But still only steady state harmonic responses are able to be analyzed by this method. To simulate nonlinear behavior of soil resistance force, Nogami et al (1991) further elaborated the previous method to model the near field soil as frequency dependent springs and dashpots in order to account for soil nonlinear behavior such as slippage and gapping. A different near-field and far-filed soil model was also published by EI Naggar and Novak (1995). The method is also capable of simulating discontinuity conditions at the pile-soil interface as well as pile-group effect.

1.4.2.2. p-y Method

The p-y method (Matlock, 1970) developed based on Beam on Winkler Foundation method, is a numerical approach to simulate the soil-structure interactions as predefined p-y curves, where p is the soil resistance (pressure per unit length of the pile) and y is the pile deflection, as shown in Figure 3. The soil is represented by a series of

nonlinear or linear p-y curves which vary with depth and soil properties. Field experiment were conducted to determine p-y curves. The method has been applied to many real problems since published, and a good ability to simulate static as well as dynamic SSI problems has been reported by former researchers.

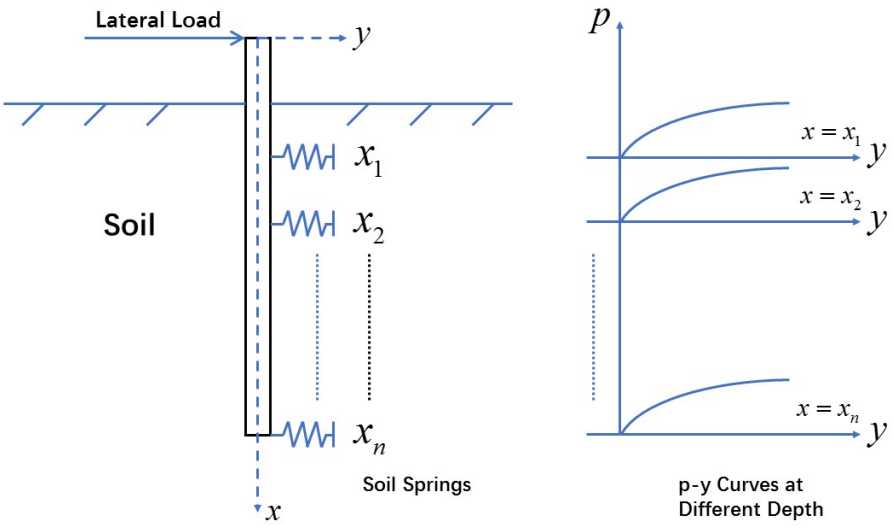

Figure 3 Laterally Loaded Single Pile

An approach combining p-y method and Newmark method was introduced by Yao et al. (2011) to simulate nonlinear behavior of super-long piles. In the research, a set of nonlinear p-y curves for clay was used to model the nonlinear SSI effect, and an optimized beam element was applied to the simulation. The results were compared with the results obtained by commercial Finite Element Analysis (FEA) software ABAQUS, and good general agreement was shown. Liang et al. (2014) corrected the commonly

used p-y curves published by Matlock (1970) to measure the relatively small soil resistance force near the mudline, and a vehicle-bridge coupled model with nonlinear lateral SSI was analyzed to determine the dynamic responses of the bridge under vehicle loads. The ability of the modified p-y curves to deal with vehicle-bridge analysis was validated. The p-y curve method has also been applied to ocean environment with a particular focus on horizontal subsea pipelines. A relatively simple nonlinear p-y curve to model the interaction between seabed soil and embedded pipe was introduced by Ai and Sun (2010), and a 2-D CFD analysis and a weak coupling fluid-structure interaction (FSI) method were performed to simulate the VIV responses of a free span pipeline. Zhu (2017) used a complex nonlinear p-y curve to model the seabed soil-pipe interactions when simulating the VIV responses of free span pipelines. In the research, a three-dimensional CFD analysis approach with overset grid was performed, and a partitioned approach to deal with FSI was adopted. Good agreement with results from previous studies was found.

1.5. Objective of Thesis

This paper presents a three-dimensional numerical method of simulating offshore riser-conductor system VIV response. The riser-conductor system is treated as a top-tensioned beam. The Soil-Structure Interactions below the mudline between conductor and surrounding soil are considered and modeled by certain p-y curves. A fully implicit discretization scheme is applied to solve the partial differential equations

which govern the pipe motion. The fluid domain above the mudline are solved numerically by Finite-Analytic Navier-Stokes (FANS) code (Chen, Patel and Ju, 1990).

In order to contribute knowledge and insight to future design and analysis of offshore drilling riser-conductor systems, simulation results from several cases are analyzed:

a) VIV simulation of a vertical pipe without SSI;

b) VIV simulations of a vertical pipe with a linear SSI model;

c) VIV simulations of a vertical pipe with a nonlinear SSI model;

d) VIV simulations with a nonlinear SSI model, but with two selected soil properties.

2. NUMERICAL METHODS

This section demonstrates the numerical methods used in riser-conductor system VIV simulations, including the Computational Fluid Dynamics (CFD) method, Soil-Structure Interaction (SSI) model, pipe motion solver, and Fluid-Structure Interaction (FSI) procedure.

2.1. Computational Fluid Dynamics Background

2.1.1. Computational Fluid Dynamics Method

In this thesis, information of the fluid domain surrounding the riser-conductor system is captured by numerically solving the unsteady, incompressible Reynolds-Averaged Navier-Stokes equations, also known as RANS equations. A CFD code, Chimera Finite-Analytic Reynolds-Averaged Navier-Stokes Program (Chen, Patel and Ju, 1990), is utilized in this research. The code has been applied to and validated in many cases by Chen et al. (2004, 2007, 2009, 2013). And a Large Eddy Simulation (LES) turbulence model is adopted in this thesis.

2.1.2. Overset Grid Approach

An overset grid meshing technique, also referred to as Chimera Grid (Meakin, 1999), is applied to mesh the fluid domain in this study.

Much effort has been paid during mesh generation process in CFD simulations, especially when the geometry of the fluid domain is complex or irregular shaped, making it hard to be represented by a single, contiguous (structured or unstructured)

grid. A possible solution to this difficulty is to use overset grid approach, in which several blocks of overlapping structured grids are constructed to represent a single complex fluid domain. Overlapping areas exist between every two neighboring blocks so that fluid information can be exchanged between them by means of interpolation. And it is worth mentioning that many grid points are not included in calculations, which are also referred to as hole points.

In general, three steps are needed to set up an overset grid simulation:

a) Grid generation;

b) Hole cutting

c) Interpolation

A cross-section of an overset grid system consists of two overlapping blocks representing a riser in a fluid domain is shown in Figure 4. The green grid block is referred to as background grids, and it is in Cartesian coordinate. The red grid block is to capture the near field of the riser boundary, and it is in polar coordinate.

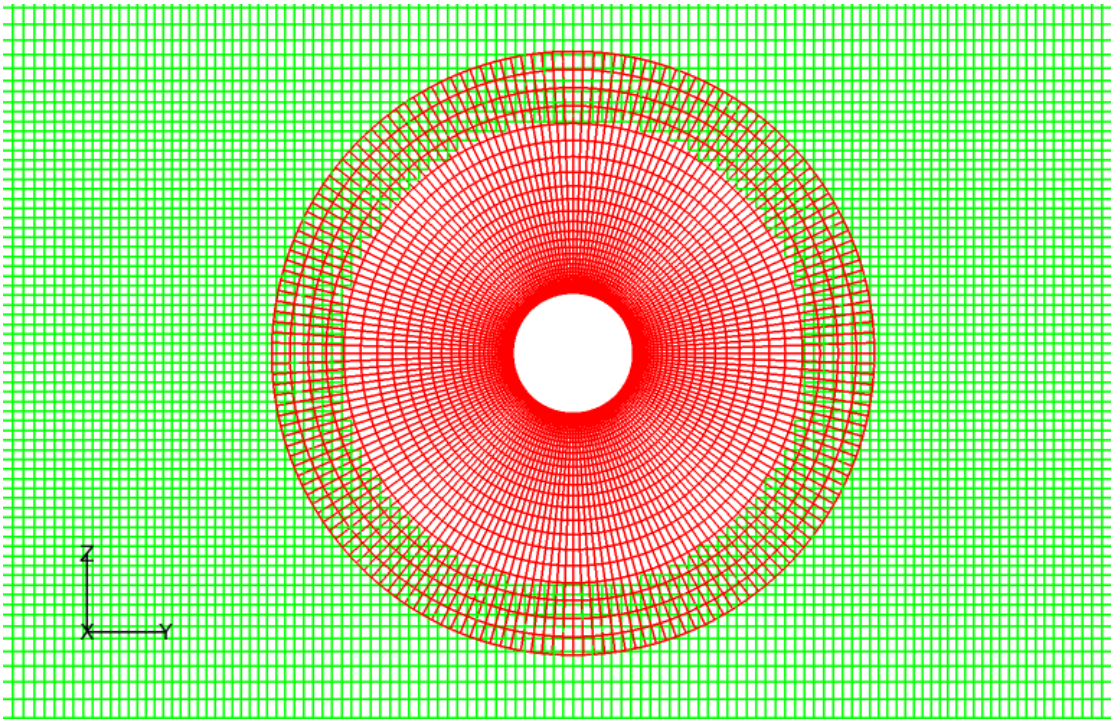

Figure 4 Overset Grid System in Riser Boundary Near Field

Much finer grids are generated near the riser outer boundary to calculate fluid in the boundary layer, while coarser grids are generated away from the riser boundary. By means of this manipulation, not only a higher resolution is reached in the near field of the riser outer boundary, but also, a significant amount of calculation time is saved due to less grid points in far field.

In this thesis, as mentioned above, two grid blocks are constructed for the simulations. The hole cutting process and interpolation of fluid information between different blocks are accomplished by NASA's PEGASUS 4.0 (Suhs and Tramel, 1991). The process of deleting points is done by firstly establishing a certain boundary in the red grid block, and then all points from background grid block (green block) located

inside that boundary will be deleted. Fluid information is interpolated and exchanged from red block points to green block points, and vice versa. Multiple geometry components within one same fluid domain, for example several risers in a same fluid domain, can also be easily generated by overset grid method. In those cases, curvilinear body-fitting grids are to be constructed for every geometry component and are to be embedded in the same background grid block.

A complete cross-section of the grid system used in this thesis is shown in Figure 5. Fine enough grids are generated for capture of vortex shedding in near region of the riser outer boundary, while coarser in other regions of the fluid domain. Again, a good balance between the resolution of the result and the calculation time is reached by means of overset grid method in this research.

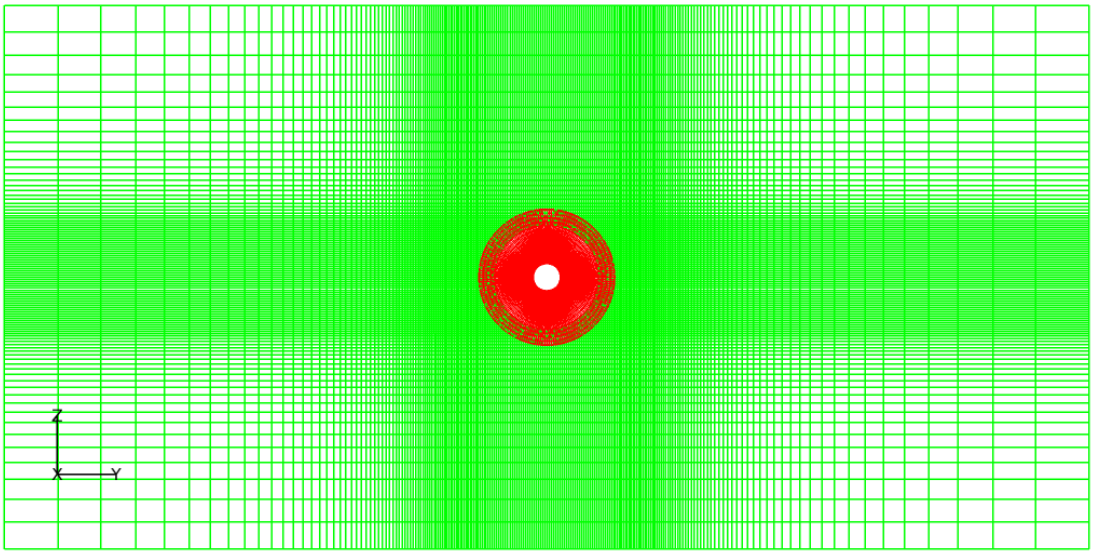

Figure 5 Cross Section of Grid System

2.1.3. Grid Generation

The computation grids for fluid domain to be used in the thesis is presented as follows. As introduced above, overset grid method is adopted in the research. Initially, two computational blocks are constructed for VIV simulations, including the near field block and the background grid (wake grid), as shown in Figure 6.

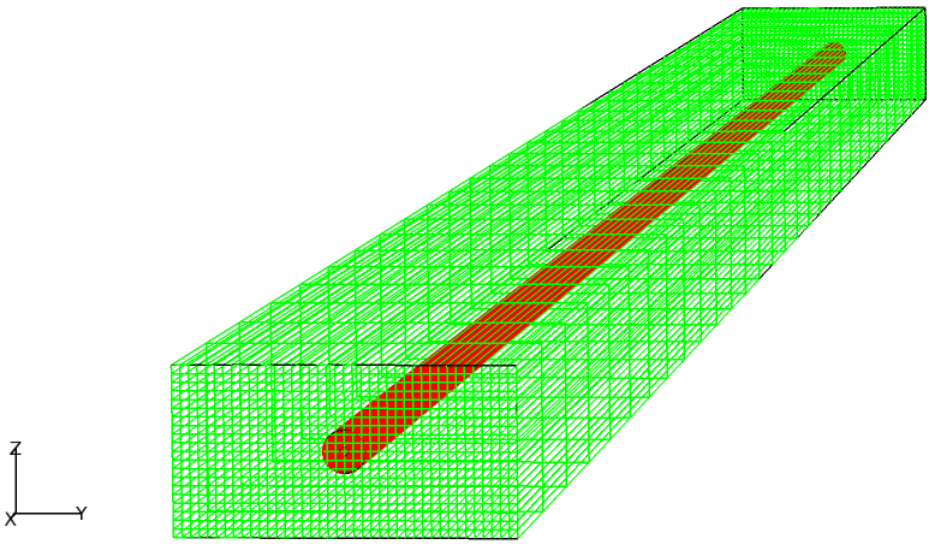

Figure 6 Overview of Initial Computational Grids

The total computational points generated in red block is 231322, with a dimension of 31×182×41. And the green block consists 629331 grid points in total, and the dimension for it is 31×201×101. Thus, a total number of approximately 0.86 million grid points are constructed for VIV simulations.

A cross-section view of the grids is shown in Figure 7. The pipe center is located at the center of the fluid domain, and is set to be the coordinate origin, which is (y, z) = (0, 0). The in-line direction, the length of the green block, is set to be 40 times pipe outer diameter. The cross-flow direction, the width of the green block, is set to be 20 times pipe outer diameter. Uniform currents parallel to the y-z plane are set to propagate from inlet to outlet direction as shown in Figure 7.

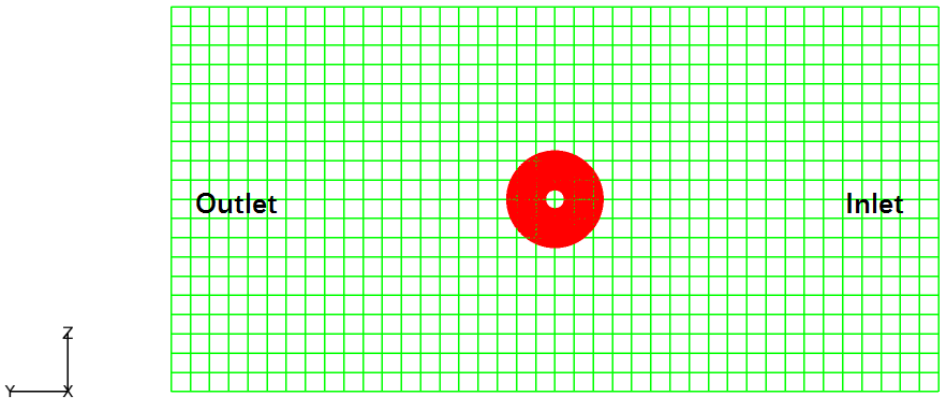

Figure 7 Cross-Section of Grids

A closer cross- section view of the red block grids is shown in Figure 8. Something need to point out is that the red block grids represent near body grids in fluid domain, instead of the pipe itself. Which means the innermost circle of the red block is the outer boundary of the pipe. In circumferential direction of the red block, 182 grid points are defined but only 180 of them are actually shown. That is because the last two

points overlap the first two points. By means of this overlapping, fluid information is able to be smoothly transformed between grid points.

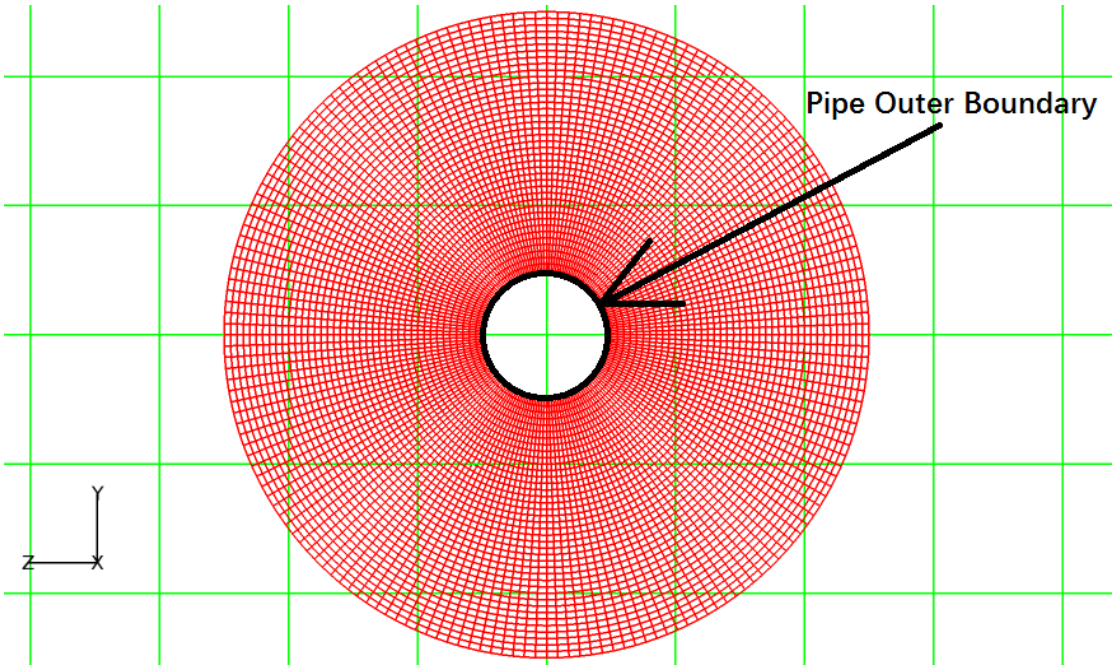

Figure 8 Pipe Outer Boundary

In the overlapping region, interpolation between grid points from different blocks is needed to exchange fluid information. To ensure a smooth information between grid blocks, grids of approximately same size in the region should be generated. However, one can tell from Figure 9 that significant grid size difference exists in overlapping region. The red block (near body block) grids are too small comparing to green block (wake block) grids. Too many red block grids exist in a single green block, grid ABCD, may result to distortion during interpolation. An ideal condition for

interpolation between different blocks is to generate grids such that only one red block grid point located inside a green block grid, in this case, grid ABCD.

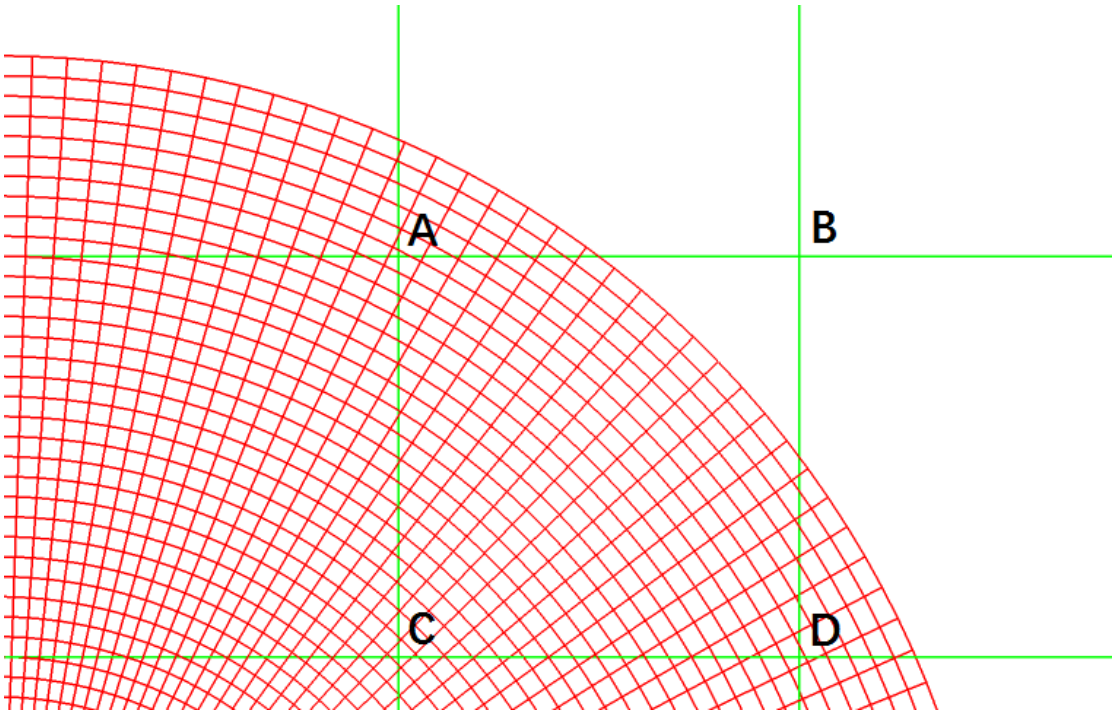

Figure 9 Interpolation between Blocks

On the other hand, very fine grid points in near field region is needed to capture fluid viscous effect including vortex generation and shedding. Nevertheless, the computation time is not acceptable if very fine grids are generated in the whole fluid domain. To balance the two key factors, grid size and computation time, such that both satisfactory resolution of results and reasonable computation time can be reached, grids adjustment is performed.

The basic concept of grids adjustment is that, in red block, generate very fine grids near the pipe boundary, and then one gradually increases the size of grids with increasing distance to the boundary. Corresponding refinement is also performed in the green block. The grids after adjustment is shown in Figure 10.

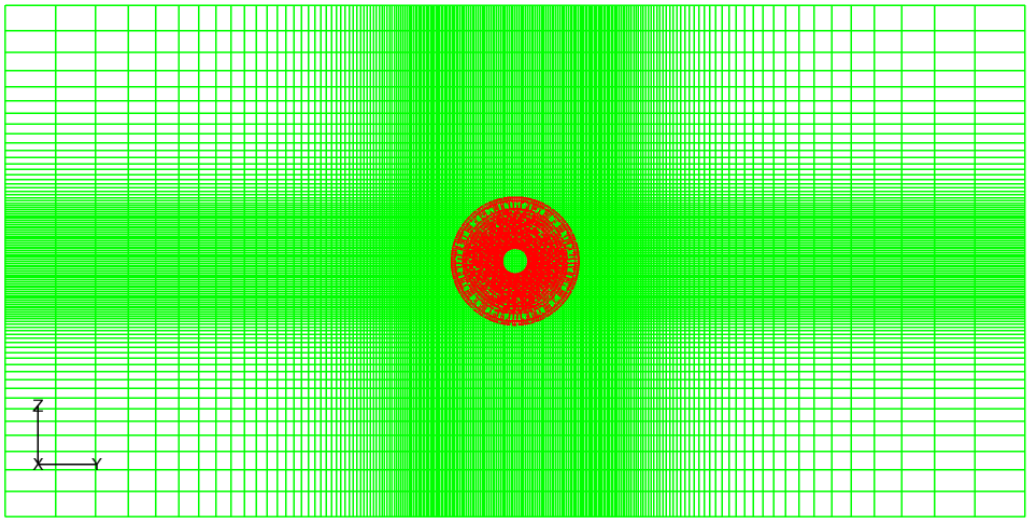

Figure 10 Grids after Adjustment

A closer look of the overlapping region is provided in Figure 11. A far better relative grid size is obtained after adjustment. Grid 1234 from red block and grid ABCD from green block are of approximately same size, thus smooth transformation of fluid information can be accomplished. As illustrated in Figure 11, fluid information of points A, B, C and D can be transformed to point 2, which is a red block grid point, by a linear interpolation. Vice versa, fluid information of point 1, 2, 3 and 4 can be transformed to point A by a similar manner.

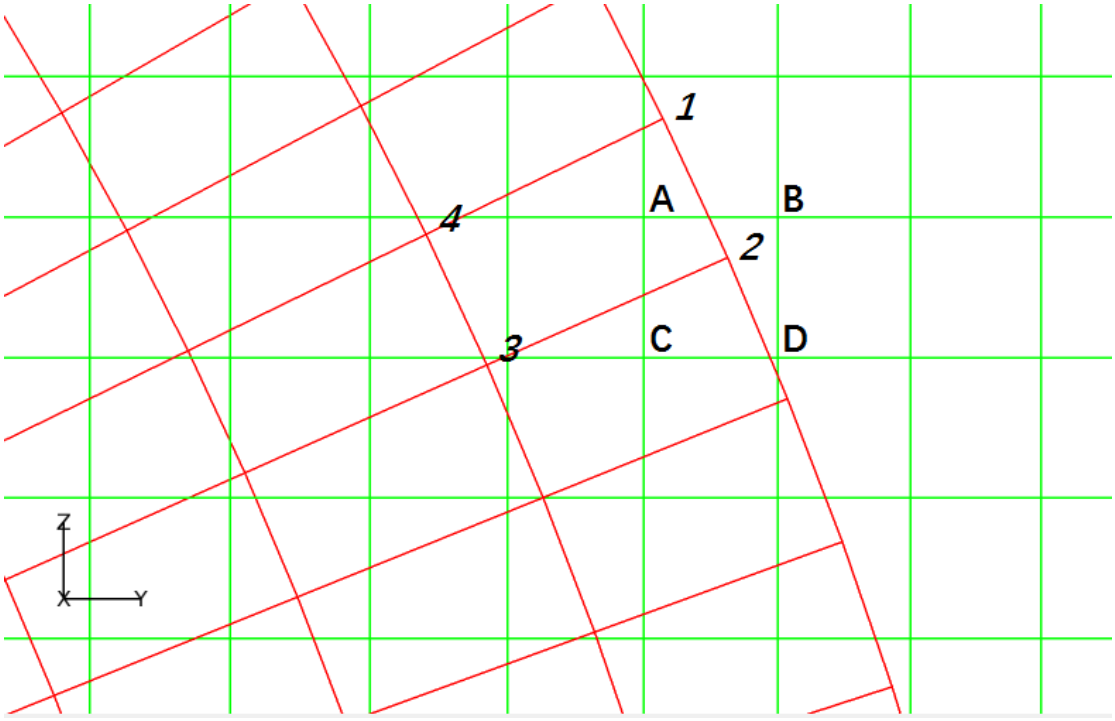

Figure 11 Interpolation after Adjustment

After the adjustment introduced above, the next thing to do is to delete green block grid points which located in the inner region of the red block, where exchange of fluid information cannot be efficiently made. Only overlapping grids in the outer region of the red block, where the sizes of green and red block grids are similar, are retained. This procedure is referred to as ‘’hole cutting’’ process as mentioned previously. The cross section of green block grids after hole cutting is shown in Figure 12 and Figure 13. A closer look of overlapping region is provided in Figure 14.

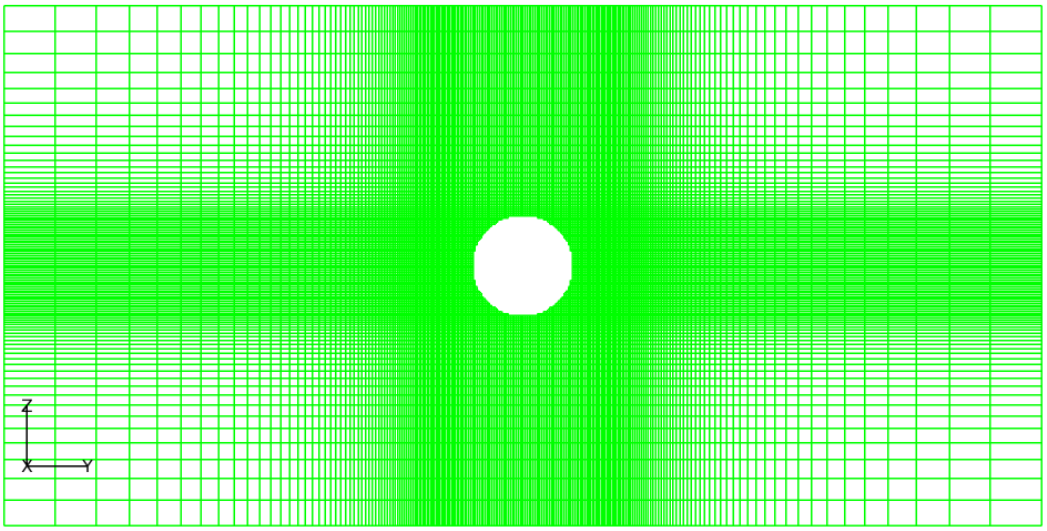

Figure 12 Green Block after Hole Cutting, Overview

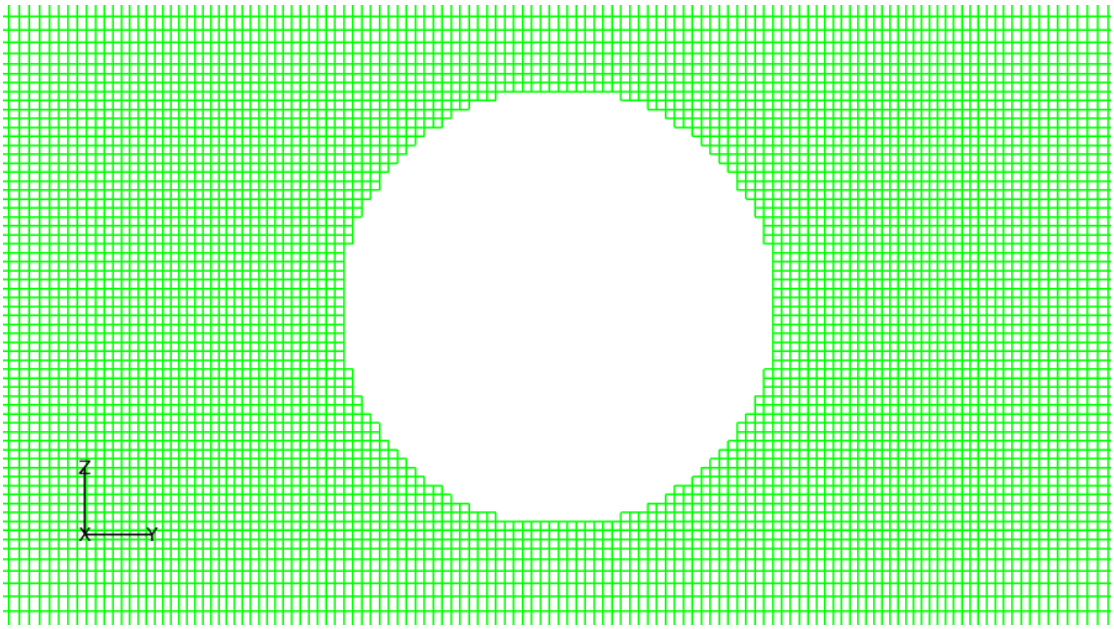

Figure 13 Green Block after Hole Cutting, Close View

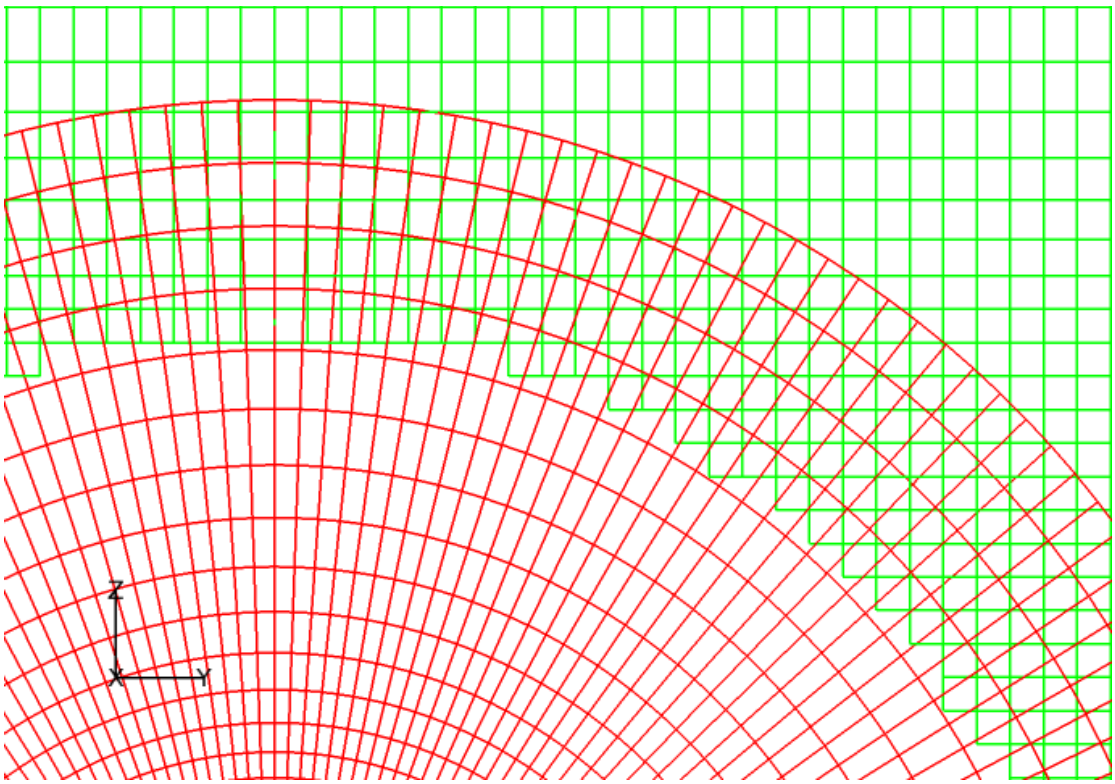

Figure 14 Overlapping Region after Hole Cutting

Finally, after all the procedures taken above, an overview of the computational grid used in this research is presented in Figure 15.

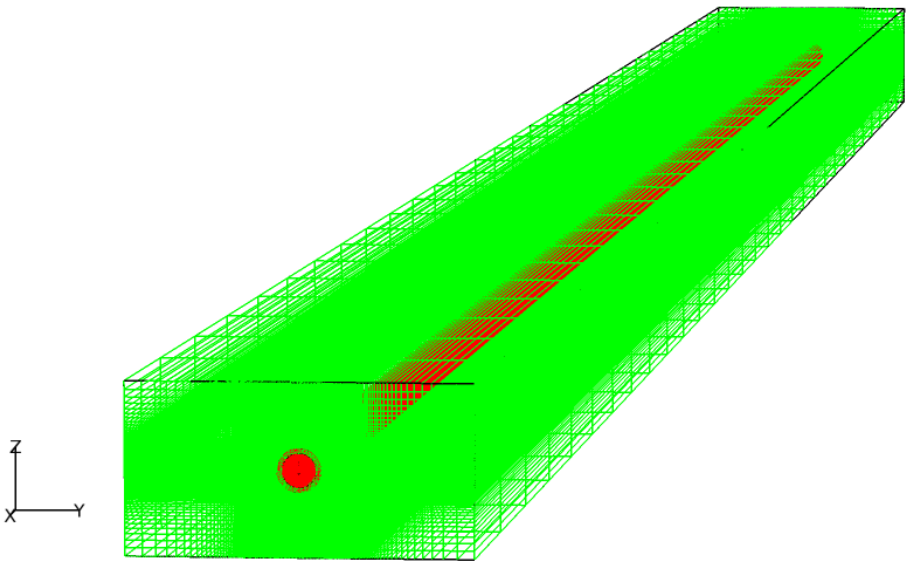

Figure 15 Final Grid

2.2. Soil-Structure Interaction (SSI) Models

The SSI models adopted in this thesis are based on the method of Beam on Winkler Foundation (Matlock and Reese, 1960; Gazetas and Dorbry, 1984). Lateral soil resistance force along the pipe is discretized to equivalent soil springs which characterized by p-y curves.

The p-y curves are based on the p-y curve for soft clay suggested by Matlock (1970), which is also adopted by API Recommended Practice 2A-WSD for the measure of soil reaction for laterally-load piles. A set of simplified Matlock curves (also referred to as linear p-y curves in following sections) and the fully nonlinear p-y curves (also referred to as nonlinear p-y curves in following sections) are used in this research.

It is worth mentioning that the "y" used in the equations which describe the SSI models represents the pipe lateral displacements, which are "y" and "z" displacements in y-z plane. And the "x" used in the equations represents the pipe axial direction.

2.2.1. Lateral Ultimate Resistance (p_u) for Soft Clay

According to Matlock (1970), following ultimate resistance per unit length of pipe is recommended:

$$p_u = \left(3c + \gamma x + J\frac{cx}{d}\right)d \quad \text{for } 0 \le x \le x_r, \tag{1}$$

$$p_u = 9cd \quad \text{for } x \ge x_r. \tag{2}$$

Where,

p_u : soil lateral ultimate resistance per unit length of pipe,

c : shear strength for soft clay,

d : diameter of pipe,

γ : effective unit weight of soft clay,

J : dimensionless empirical constant with values from 0.25 to 0.5, and value of 0.5 is suggested for Gulf of Mexico clays,

x : depth below soil surface,

x_r : depth of reduced resistance, given as:

$$x_r = \frac{6d}{\frac{\gamma d}{c} + J} \tag{3}$$

The curve describing the change of soil ultimate resistance p_u with soil depth is shown in Figure 4.

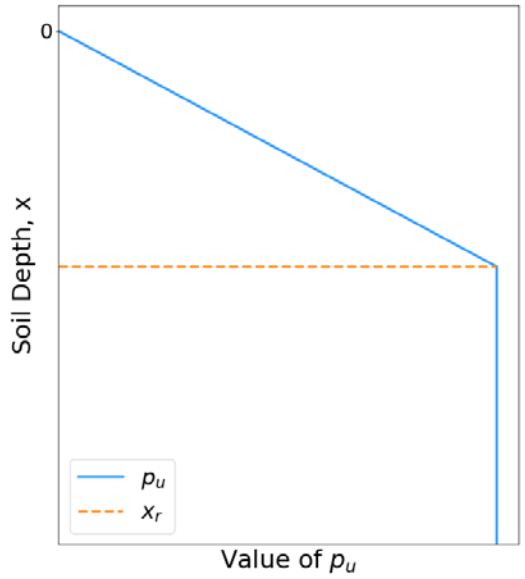

Figure 16 p_u versus soil depth

2.2.2. Nonlinear p-y Curves for Soft Clay

The proposed load-deflection (p-y) curves for soft clay is shown in Figure 17. The ordinate is normalized by p_u, and the abscissa is normalized by y_c, which is given by:

$$y_c = 2.5\varepsilon_c d \tag{4}$$

where ε_c is the strain which occurs at one-half of the maximum stress on laboratory sample test. A value of 0.010 is suggested by Matlock (1970) for most purposes.

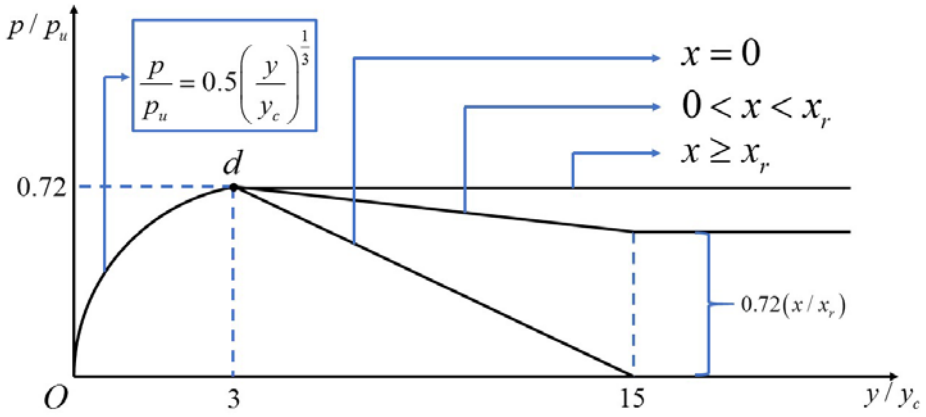

Figure 17 p-y curves for soft clay

When the deflection of the pipe is less than 3 times y_c, that is to say $y/y_c \le 3$, the p-y curve is described as

$$\frac{p}{p_u} = 0.5\left(\frac{y}{y_c}\right)^{\frac{1}{3}} \tag{5}$$

For soil at the free surface, which is $x = 0$, complete loss of soil resistance is assumed when $y/y_c \ge 15$. For soil in the range from free soil surface and depth of reduced resistance, which is $0 \le x \le x_r$, a constant value of resistance force is given as $y/y_c \ge 15$:

$$\frac{p}{p_u} = 0.72\left(\frac{x}{x_r}\right) \tag{6}$$

For soil below the depth of reduced resistance, $x \geq x_r$, maximum soil resistance of 0.72 p_u is reached at $y / y_c = 3$.

2.2.3. Simplified p-y Curves for Soft Clay

The nonlinear p-y curve shown in Figure 17 is nonlinear in lateral directions. In an effort to logically and clearly analyze the effect of different SSI models on VIV simulations of riser-conductor system, one simplified p-y curve based on the fully nonlinear p-y curve is presented and used for VIV simulation first.

The simplification is made only for the relation between p / p_u and y / y_c. Which means, the equations describing the relation between p_u and soil depths is still given by Eq. (1) and Eq. (2), and the general nature of that relation is still represented by Figure 16.

In lateral directions, a simplified linear p-y relation is shown in Figure 18. The line is defined by linking points O and point d in Figure 17 directly, and is given as:

$$\frac{p}{p_u} = 0.24\left(\frac{y}{y_c}\right) \tag{7}$$

In other words, the nonlinearity of soil resistance with lateral displacement and the modification of free soil surface ($x = 0$) are ignored.

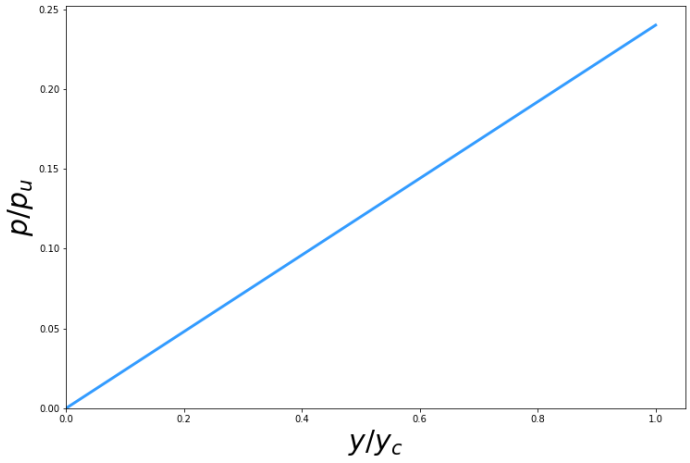

Figure 18 Simplified p-y Curve

2.3. Pipe Motion Solver

2.3.1. Governing Equations

A deepwater drilling riser-conductor systems can be simplified as a top tensioned beam with in-line and cross-stream motions. The partial deferential equations which govern its lateral motion are as follows:

$$T\frac{d^2y}{dx^2}+\frac{dy}{dx}\frac{dT}{dx}-\frac{d^2}{dx^2}\left(EI\frac{d^2y}{dx^2}\right)+f_y=m\ddot{y}+D_S\dot{y} \tag{8}$$

$$T\frac{d^2z}{dx^2}+\frac{dz}{dx}\frac{dT}{dx}-\frac{d^2}{dx^2}\left(EI\frac{d^2z}{dx^2}\right)+f_z=m\ddot{z}+D_S\dot{z} \tag{9}$$

The x in the above equations represents the pipe axial direction, which is vertical to the ground; y and z denote the in-line and cross-flow directions, respectively. E and I are Young's modulus and the area moment of inertia of the pipe,

while m and D_S denote the mass per unit length and damping coefficient of the pipe. f_y and f_z represent the external forces of corresponding directions.

The governing equations of pipe motions are partial differential equations (PDE) with a fourth-order derivative in space and a second-order derivative in time. The finite difference method can be applied to discretize each of the terms in Eq. (1), as follows:

$$\frac{dy}{dx} = \frac{-3y_i^n + 4y_{i+1}^n - y_{i+2}^n}{2\Delta x} \quad \text{for} \quad i = 1, \tag{10}$$

$$\frac{dy}{dx} = \frac{y_{i+1}^n - y_{i-1}^n}{2\Delta x} \quad \text{for} \quad i = 2 \cdots N-1, \tag{11}$$

$$\frac{dy}{dx} = \frac{y_{i-2}^n - 4y_{i-1}^n + 3y_i^n}{2\Delta x} \quad \text{for} \quad i = N, \tag{12}$$

$$\frac{d^2y}{dx^2} = \frac{y_{i+2}^n - 2y_{i+1}^n + y_i^n}{(\Delta x)^2} \quad \text{for} \quad i = 1, \tag{13}$$

$$\frac{d^2y}{dx^2} = \frac{y_{i+1}^n - 2y_i^n + y_{i-1}^n}{(\Delta x)^2} \quad \text{for} \quad i = 2, \cdots, N-1, \tag{14}$$

$$\frac{d^2y}{dx^2} = \frac{y_i^n - 2y_{i-1}^n + y_{i-2}^n}{(\Delta x)^2} \quad \text{for} \quad i = N, \tag{15}$$

$$\frac{d^4y}{dx^4} = \frac{y_{i+4}^n - 4y_{i+3}^n + 6y_{i+2}^n - 4y_{i+1}^n + y_i^n}{(\Delta x)^4} \quad \text{for} \quad i = 1, \tag{16}$$

$$\frac{d^4y}{dx^4} = \frac{y_{i+3}^n - 4y_{i+2}^n + 6y_{i+1}^n - 4y_i^n + y_{i-1}^n}{(\Delta x)^4} \quad \text{for} \quad i = 2, \tag{17}$$

$$\frac{d^4y}{dx^4} = \frac{y_{i+2}^n - 4y_{i+1}^n + 6y_i^n - 4y_{i-1}^n + y_{i-2}^n}{(\Delta x)^4} \quad \text{for} \quad i = 3, \cdots, N-2, \tag{18}$$

$$\frac{d^4y}{dx^4} = \frac{y_{i-3}^n - 4y_{i-2}^n + 6y_{i-1}^n - 4y_i^n + y_{i+1}^n}{(\Delta x)^4} \quad \text{for} \quad i = N-1, \tag{19}$$

$$\frac{d^4y}{dx^4} = \frac{y_{i-4}^n - 4y_{i-3}^n + 6y_{i-2}^n - 4y_{i-1}^n + y_i^n}{(\Delta x)^4} \quad \text{for} \quad i = N, \tag{20}$$

$$\frac{dy}{dt} = \frac{y_i^n - y_i^{n-1}}{\Delta t} \quad \text{for} \quad i \geq 2, \tag{21}$$

$$\frac{d^2y}{dt^2} = \frac{y_i^n - 2y_i^{n-1} + y_i^{n-2}}{(\Delta t)^2} \quad \text{for} \quad i \geq 3. \tag{22}$$

Discretized governing equation for in-line motion now can be given as:

$$\begin{aligned} &\frac{EI}{(\Delta x)^4} y_{i-2}^n - \left(\frac{T_i}{(\Delta x)^2} - \frac{1}{2\Delta x}\frac{dT_i}{dx} + \frac{4EI}{(\Delta x)^4} \right) y_{i-1}^n + \left(\frac{2T_i}{(\Delta x)^2} + \frac{6EI}{(\Delta x)^4} + \frac{m}{(\Delta t)^2} + \frac{D_S}{\Delta t} \right) y_i^n \\ &- \left(\frac{T_i}{(\Delta x)^2} + \frac{1}{2\Delta x}\frac{dT_i}{dx} + \frac{4EI}{(\Delta x)^4} \right) y_{i+1}^n + \frac{EI}{(\Delta x)^4} y_{i+2}^n \\ &= f_{yi}^n + \left(\frac{2m}{(\Delta t)^2} + \frac{D_S}{\Delta t} \right) y_i^{n-1} - \frac{m}{(\Delta t)^2} y_i^{n-2} \end{aligned} \tag{23}$$

A similar manner can be used to derive the discretized governing equation for cross-flow motion:

$$\begin{aligned} &\frac{EI}{(\Delta x)^4} z_{i-2}^n - \left(\frac{T_i}{(\Delta x)^2} - \frac{1}{2\Delta x}\frac{dT_i}{dx} + \frac{4EI}{(\Delta x)^4} \right) z_{i-1}^n + \left(\frac{2T_i}{(\Delta x)^2} + \frac{6EI}{(\Delta x)^4} + \frac{m}{(\Delta t)^2} + \frac{D_S}{\Delta t} \right) z_i^n \\ &- \left(\frac{T_i}{(\Delta x)^2} + \frac{1}{2\Delta x}\frac{dT_i}{dx} + \frac{4EI}{(\Delta x)^4} \right) z_{i+1}^n + \frac{EI}{(\Delta x)^4} z_{i+2}^n \\ &= f_{zi}^n + \left(\frac{2m}{(\Delta t)^2} + \frac{D_S}{\Delta t} \right) z_i^{n-1} - \frac{m}{(\Delta t)^2} z_i^{n-2} \end{aligned} \tag{24}$$

Where Δx and m are element length and mass of the pipe, respectively; Δt is the time step in the simulation; n denotes the current time step, while T represents the top tension experienced by the pipe. Other pipe parameters, E, I, D_S are also predefined

in the simulations. External forces f_y and f_z are obtained by adding soil force and fluid force every time step. Therefore, the only unknowns in the finite difference governing equations are pipe displacements in in-line and cross-flow directions.

2.3.2. Validation of Pipeline Motion Solver

The pipe motion solver has been validated by Huang and Chen (2011), and Xiao (2015). It is verified in this thesis again for the primary purpose to validate the Soil-Structure Interaction models.

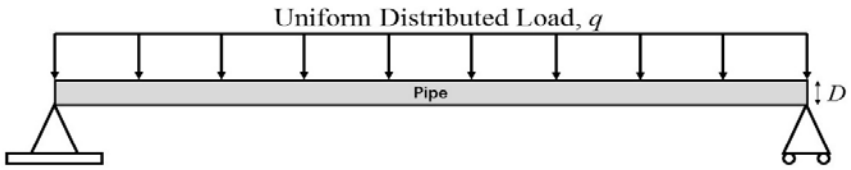

Figure 19 Uniform Distributed Load on Pipe

The motion solver is verified by comparing with analytic solutions in two cases: 1) a riser with constant pretension under uniform distributed loads, as shown in Figure 19; 2) a riser with linear tension distribution, a non-zero tension gradient, under uniform

distributed loads. In real ocean environment, the highest tension occurs at the top of the system, while the lowest occurs at the bottom due to the weight of the pipe itself.

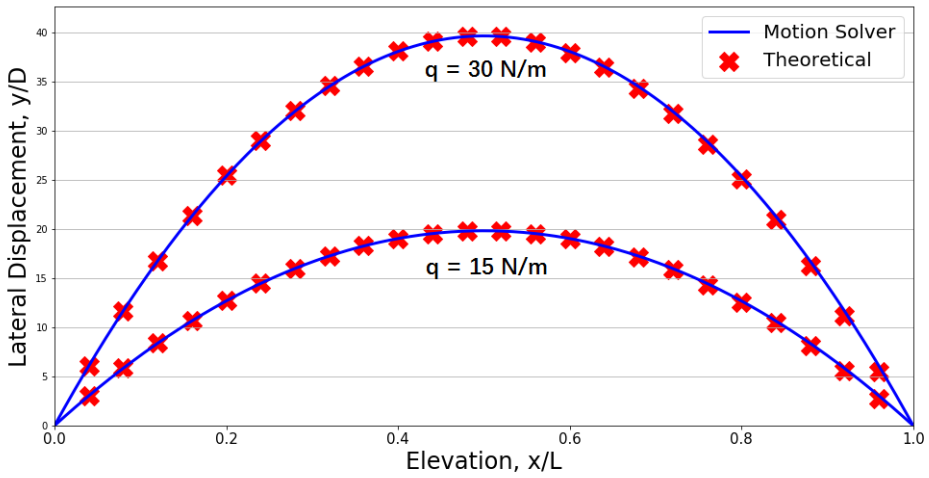

Figure 20 Uniform Distributed Loads, Uniform Tension

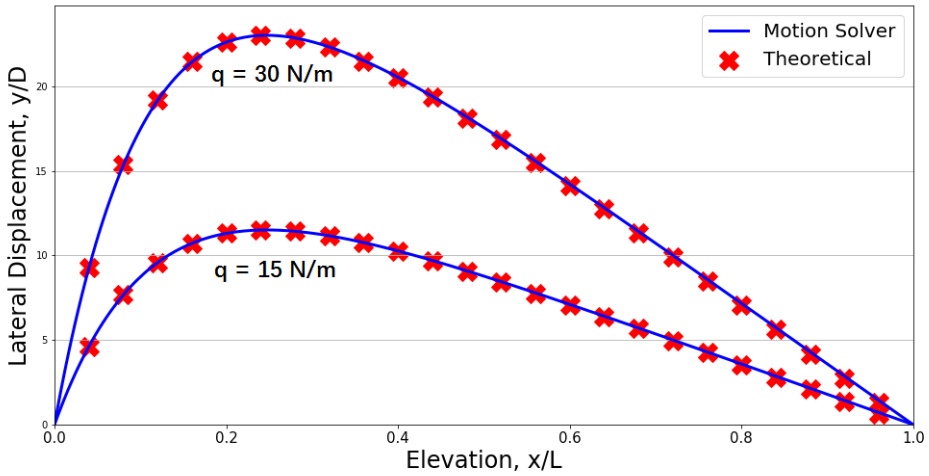

Figure 21 Uniform Distributed Loads, Distributed Tension

The results are shown above in Figure 20 and 21. For the first case, the lateral displacement of pipe is symmetric about the middle of the pipe, at which the maximum displacement occurs. To the contrast, for the second case, lateral displacement is non-symmetric and the maximum displacement occurs at the lower portion of the pipe. For both cases, motion solver solution and the theoretical solution coincide.

2.3.3. Validation of Soil-Structure Interaction Model

To validate the SSI model used in this research, the linear p-y curve introduced in 3.2.3 is verified in a static load case by comparing the obtained result from the motion solver with the published analytical and Finite Element Analysis (FEA) solutions (Choi and Basu, 2013).

The case is illustrated in Figure 22. A pipe with total length of 15m is discretized to 250 segments with 251 computation nodes, that is to say, a mesh length (Δx) of 0.06 m is used for this case. A lateral load of 300kN is applied to the first node of the pipe. Soil springs are added to every node of the pipe inside soil to model the later soil resistance force, and both ends of the pipe are set free.

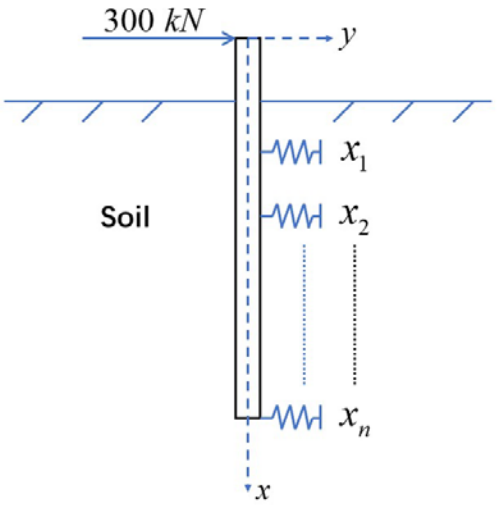

Figure 22 Case Illustration

The p-y curves which characterize the soil resistance force are calculated by Eq. (1), (2), (3), and (7). It is worth mentioning that the soil lateral ultimate resistance, p_u, is linearly increasing with soil depth until the soil depth reaches the depth of reduced resistance, x_r, which in this case is 4.32 m. Therefore, soil resistance is of its lowest value at the free-soil surface, the #1 computation node, and increasing to its maximum value at depth of reduced resistance, the #73 computation node. The parameters used in this case are according to the case published by Choi and Basu (2013) as listed in table 1.

Table 1 Parameters for Validation

Parameter	**Units**	**Value**
Pipe Diameter, d	m	0.6
Soil Shear Strength, c	kPa	36
Soil Effective Unit Weight, γ	N / m^3	20000
Strain of Half Maximum Stress, ε_c	1	0.01
Empirical Constant, J	1	0.5

Results obtained from the pipe motion solver used in this research are compared with the results obtained by Choi and Basu (2013), as shown in Figure 23. A good agreement of pipe lateral displacement is shown between present solution and published solutions: the key feature of a negative displacement of the pipe between approximately soil depth of 3m to 8m is captured. The difference between results calculated by the motion solver and the published research is less than 15%. Therefore, the efficiency of the Soil-Structure Interaction model as well as the motion solver is validated.

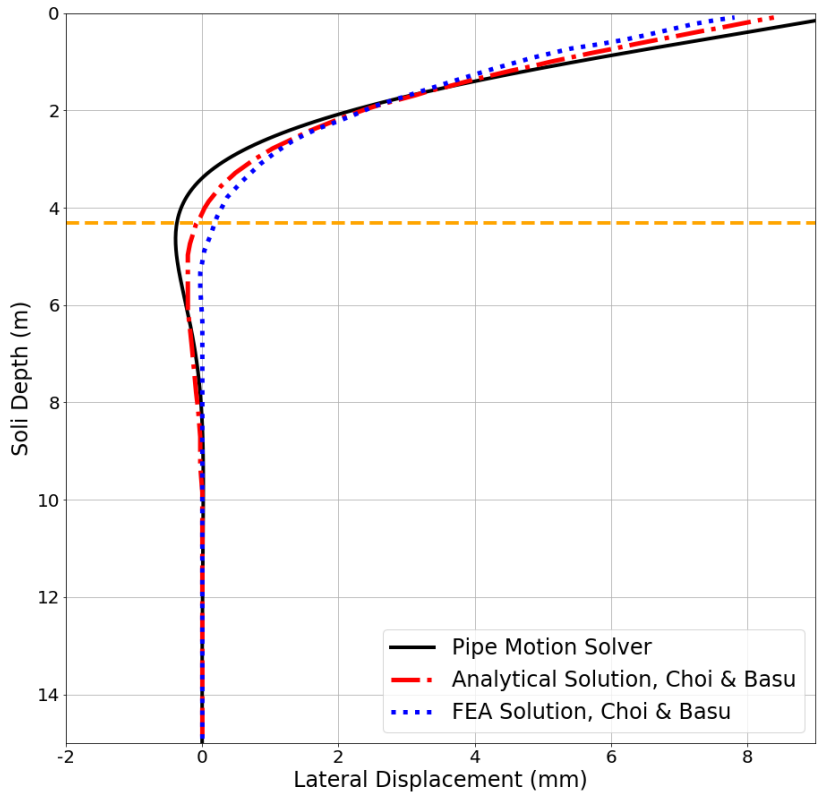

Figure 23 Comparison with Published Solutions

A set of experiments is conducted to ensure that the result presented above is accurate enough, which means that the increase of the number of computation points does not increase the resolution of the result significantly. As shown in Figure 24, when 125 or more computation points are used, the results are not significantly different. Thus, the use of 250 points with the element length of 0.06 m is fine enough for computation.

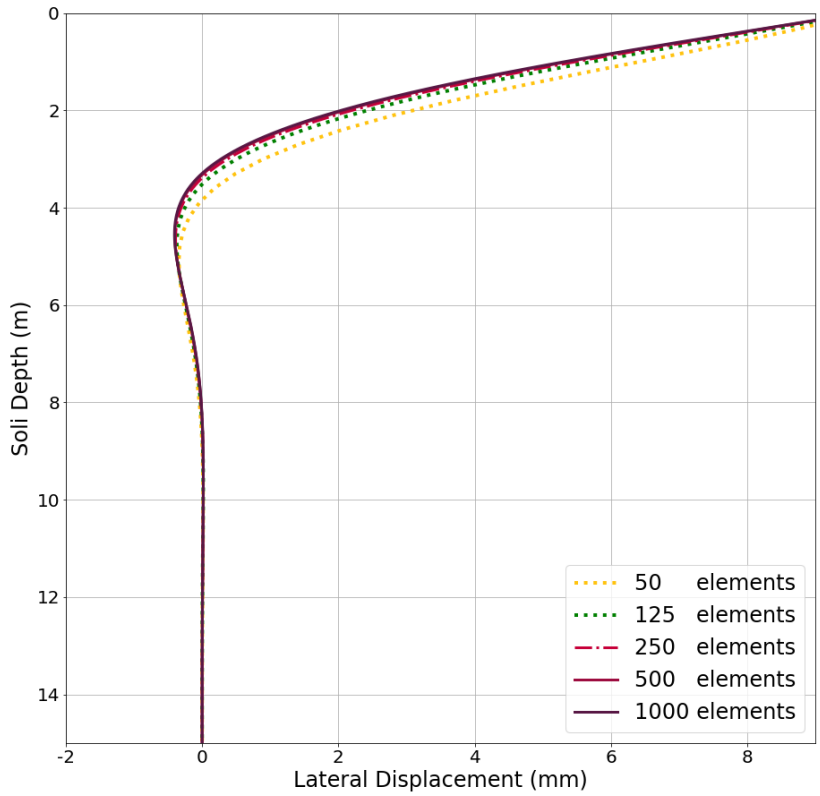

Figure 24 Resolution Check

2.4. Fluid-Structure Interaction Procedure

In the study of VIV response of riser-conductor system, the pipe will deform and move under fluid force. In the other way around, the fluid domain will be affected due to the change of the pipe outer boundary position. This kind of problem is known as Fluid-Structure Interaction (FSI) problems. Two main approaches exist for dealing with FSI problems, which are monolithic approach and partitioned approach. The monolithic approach is a strong coupling method, in which the fluid and structure motion equations

are represented as a single matrix system and is solved together by a certain solver at every time step. The partitioned approach, on the other hand, a method of solving fluid domain and structure motion separately, is a weak coupling process.

The FSI method adopted in this research is the partitioned approach, in which the existing fluid domain solver, FANS, can be fully utilized by coupling with the pipe motion solver presented above. The FSI procedure is accomplished by the following manner: At every time step, Filtered (volume-averaged) Navier-Stokes equations are numerically solved first thus the fluid force on the pipe surface is able to be calculated and prepared for the motion solver. After that, pipe motion solver is called as a subroutine to solve the pipe displacement and velocity. Once pipe displacement and velocity are obtained, new fluid domain grids can be generated and new boundary conditions are prepared for the fluid solver for next time step calculation. The basic idea of partitioned FSI approach in this thesis is illustrated in Figure 25.

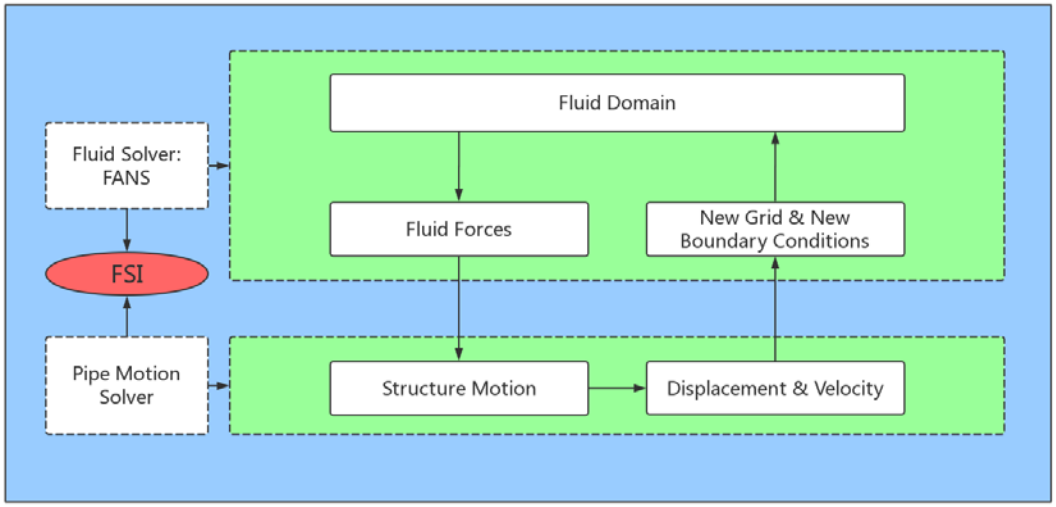

Figure 25 FSI Procedure

It is also worth mentioning that in axial direction, x direction in this research, much coarser grid is used for fluid domain computation, whereas finer grid is used for structure motion computation. By the facts that fluid information does not vary as significant as structure motion in the axial direction and the pipe motion solver is much faster than the fluid solver, 30 computational segments in fluid domain and more than 200 segments in structure motion calculation are used. Force and displacement information obtained from each solver is exchanged by means of interpolation.

3. BENCHMARK CASE: VIV SIMULATION OF A VERTICAL PIPE WITHOUT CONSIDERING SOIL-STRUCTURE INTERACTIONS

3.1. Description

In order to logically study the VIV responses of riser-conductor systems with considering the soil-structure interactions (SSI), a VIV simulation of a vertical pipe without considering SSI is firstly analyzed, which will also be served as a benchmark case for this research

In this simulation, a pipe with aspect ratio (length to diameter) of 482.5 is analyzed. The pipe vertically stands in the fluid field, and both ends of the pipe are pinned, that is to say, no lateral displacement at two ends are allowed. A linear distributed tension is used since the pipe is vertically standing in the fluid, largest tension will show at the top of the pipe due to the submerged weight of itself

A similar case with different computation grids has been studied and discussed by Xiao (2015). In his thesis, numerical results were compared with experiment results to verify the efficiency of FANS code in pipe VIV simulations, and good agreement was shown. Therefore, the comparison between numerical solution and experimental data is not provided in this thesis. The primary concern of this research is the SSI effect in pipe VIV simulations, data collected from this case will be served as a benchmark and be used to compare with the pipe VIV simulations including SSI.

The grid generation process has been discussed in detail in previous sections. Necessary pipe parameters are listed as follows in Table 2.

Table 2 Pipe Parameters

Parameter	Units	Value
Pipe Diameter	m	0.3
Pipe Length	m	144.45
Bending Stiffness	$N \cdot m^2$	6.85E6
Top Pretension	N	1.84E5
Bottom Pretension	N	1.75E5

3.2. Simulation Results

3.2.1. Fluid Domain

A uniform current with flow speed of 0.42 m/s is applied to this simulation. A cross section of the computation domain is selected to describe this simulation. In this simulation, vortex generation process is observed in the early stage of the simulation within the time step range of roughly 0 to 3000, as shown in Figure 26.

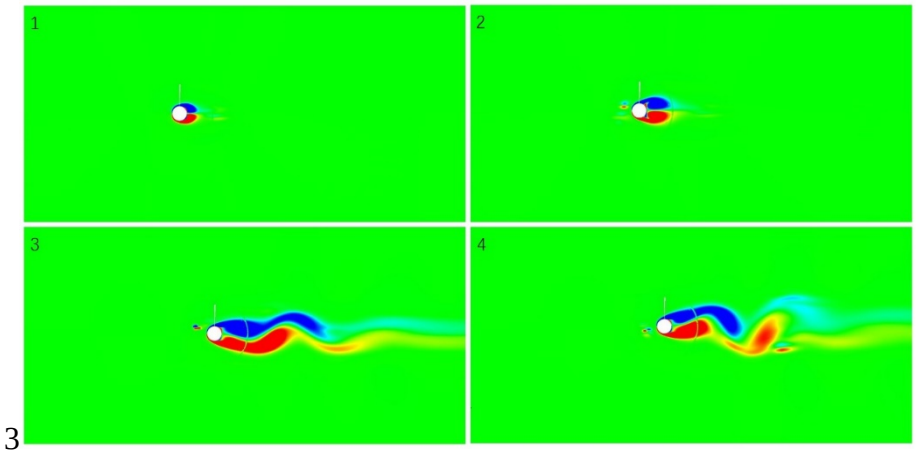

3

Figure 26 Vortex Generation Process, Benchmark

Then, vortex shedding phenomenon occurs on the pipe outer surface. Generated vortexes from pipe surface boundary layer start to detach from the pipe outer surface and make the pipe oscillate in the cross-flow direction. On the other hand, vibrating pipe affects the fluid field as well. From time step 5000, a nearly periodic state is shown in the fluid field. Vortex generates and detaches from the pipe outer surface regularly under certain frequencies. The fluid field within this time step range is shown in Figure 27. For better understanding the complete fluid domain, selected cross-sections of two specific time steps are provided in Figure 28.

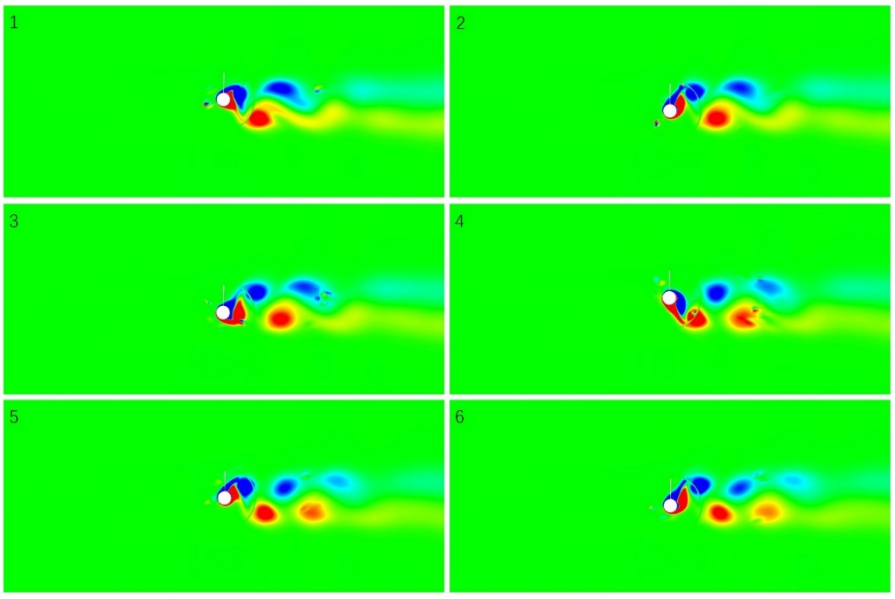

Figure 27 Vortex Shedding, Benchmark

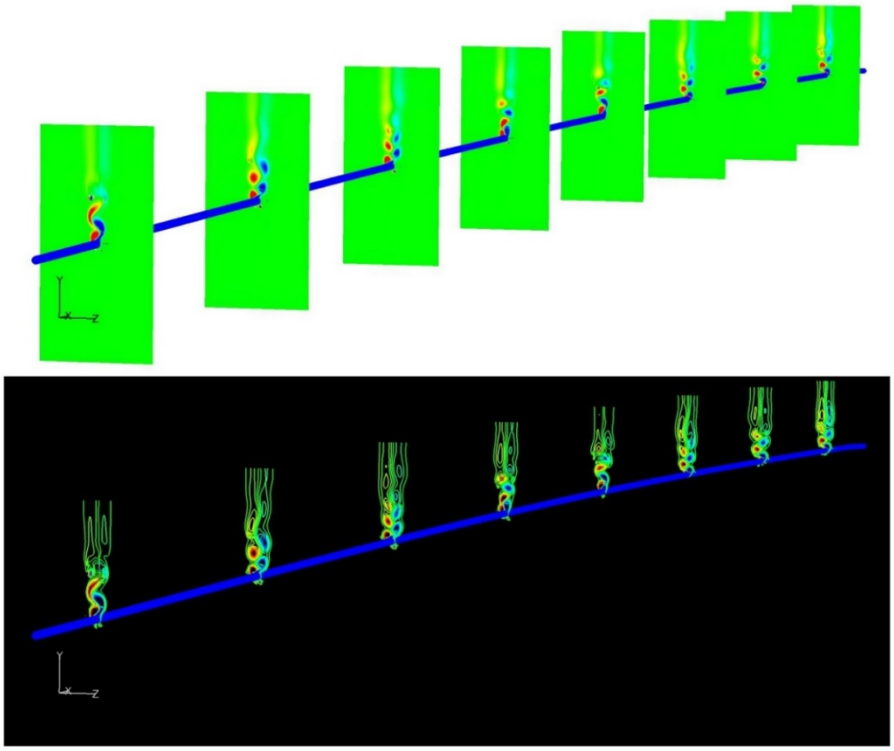

Figure 28 Fluid Domain View, Benchmark

3.2.2. Pipe Motion History

Pipe motion history for a pipe middle cross-section in in-line and cross-flow directions are presented in Figure 29 and Figure 30, respectively. Note that the displacement is normalized by the pipe diameter, 20 mm. As shown in the Figure 29, the pipe starts to deflect quickly in the in-line direction at the beginning of the simulation, and then the curve drops to about 1.5 pipe diameter at time step 2500 due to the bending stiffness of the pipe itself. After that, the pipe continues to deflect in the in-line direction until it reaches a nearly periodic state, oscillating in the range of 2.5 to 4.0 pipe

diameters starting from about 7500 time step. The maximum value of the pipe in-line deflection is approximately 4.0 times pipe diameter.

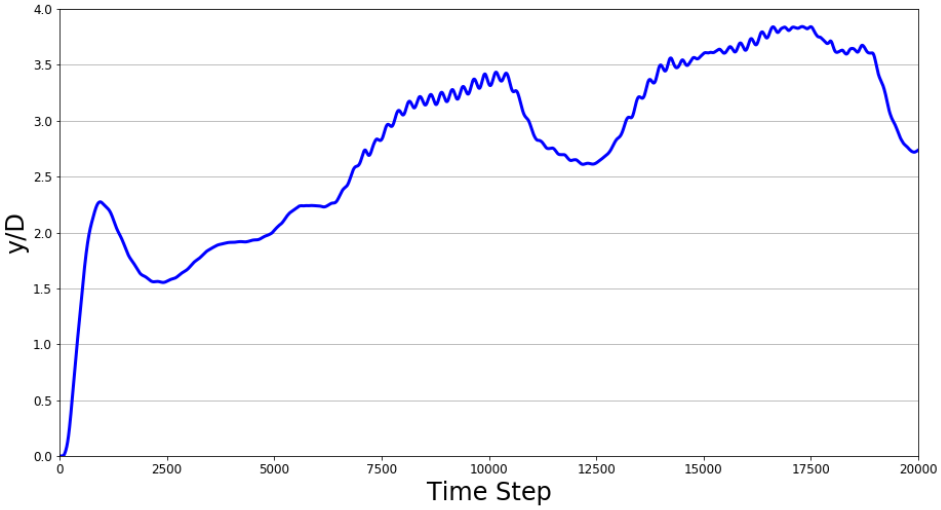

Figure 29 Pipe Stream Wise Motion, Benchmark

For the cross-flow direction as shown below, no significant deflection is shown until time step 2500. The reason for this is that vortex has not shed regularly from the pipe surface before this time. A nearly periodic state with large amplitude vibrations is shown after time step 5000, which is also referred to as vortex-induced vibration (VIV), and the maximum cross-flow displacement is about 0.8 pipe diameters.

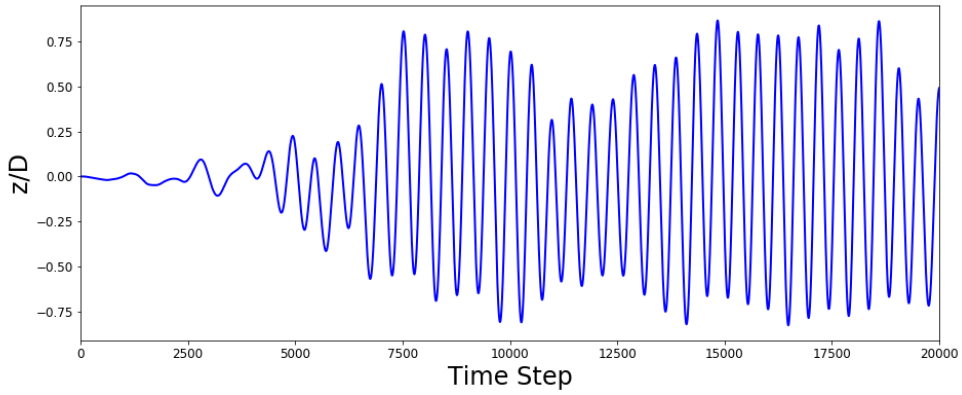

Figure 30 Pipe Cross-Flow Motion, Benchmark

Trajectory of the pipe is thus obtained, as shown in Figure 31. A clear pipe VIV response pattern deformed “8” is captured, as shown in Figure 32. The pipe deflects in the in-line direction first and starts to vibrate in the cross-flow direction. Fast-Fourier Transformation (FFT) is applied to the cross-flow response of the same cross-section, as shown in Figure 33. The peak occurs roughly at 4 Hz, which is in good agreement of analytical value of vortex shedding frequency.

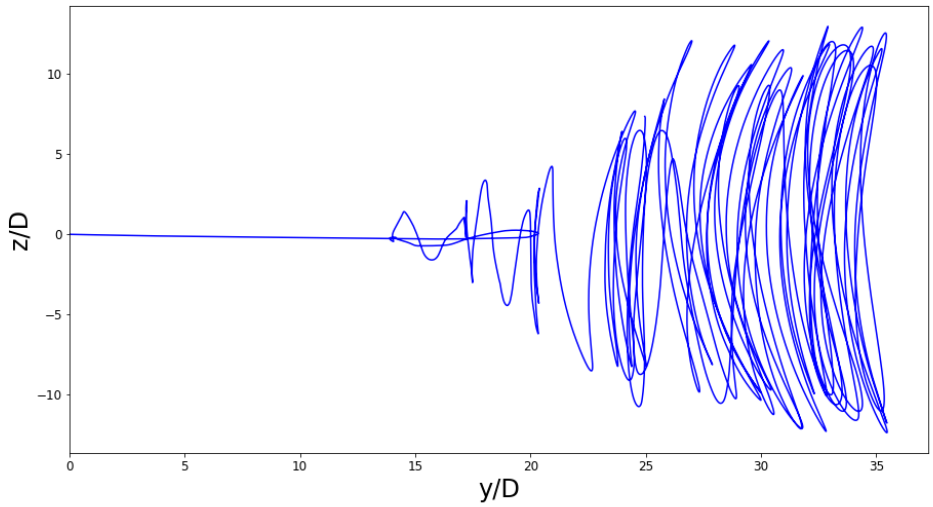

Figure 31 Pipe Trajectory, Benchmark

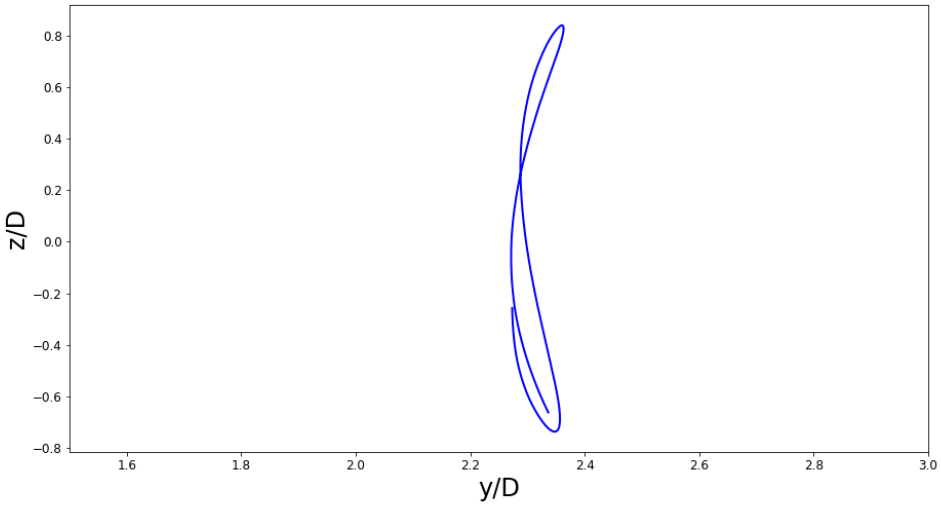

Figure 32 Trajectory, Selected Time Steps, Benchmark

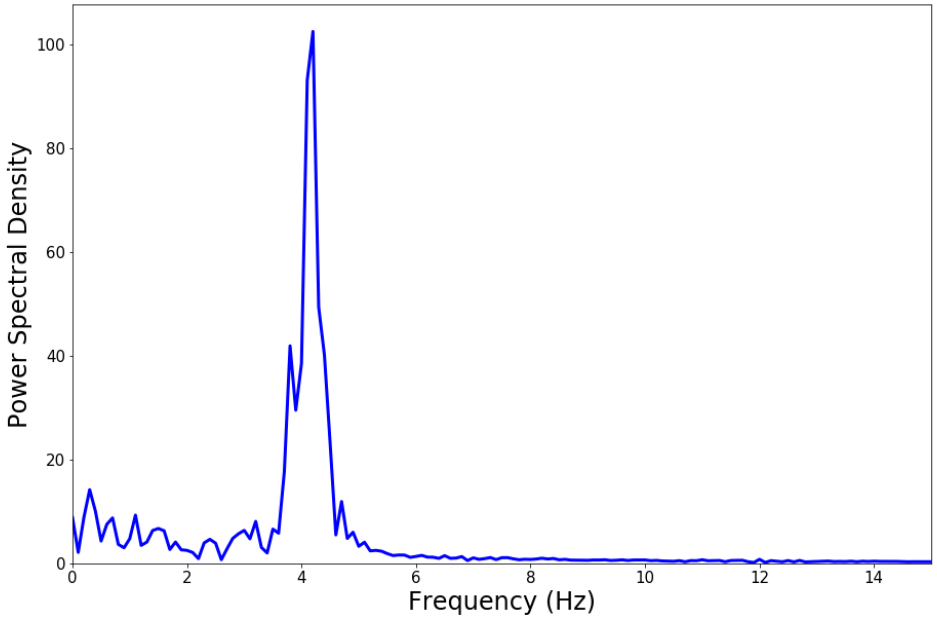

Figure 33 Spectrum, Benchmark

Above analysis are based on one certain cross-section of the pipe. For a better understanding of the full pipe, an in-line displacement plot and a cross-flow displacement plot of all pipe nodes with increasing time steps are provided in Figure 34 and Figure 35, respectively. The ordinates of these two plots are pipe computation nodes, which are from point 1 to point 251. Which means the pipe is divided into 250 segments in the computation. The points in the plot are colored by their displacement (normalized by pipe diameter).

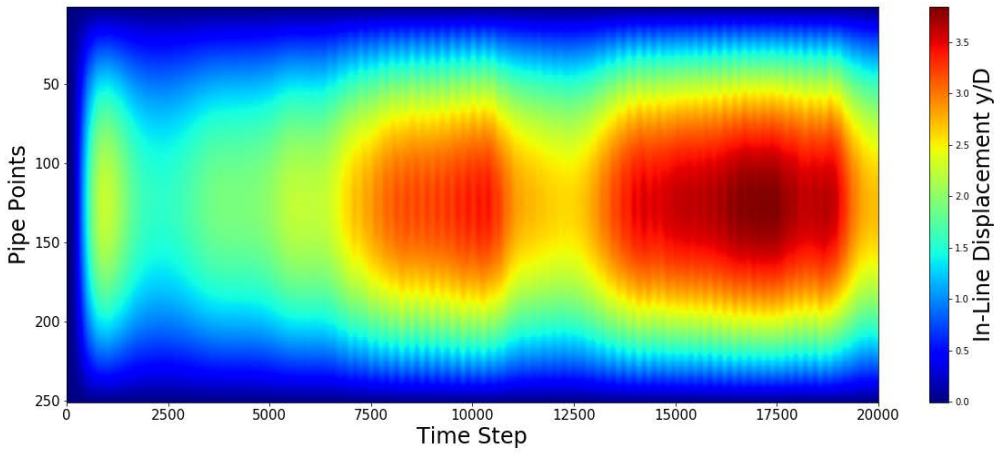

Figure 34 In-Line History, Benchmark

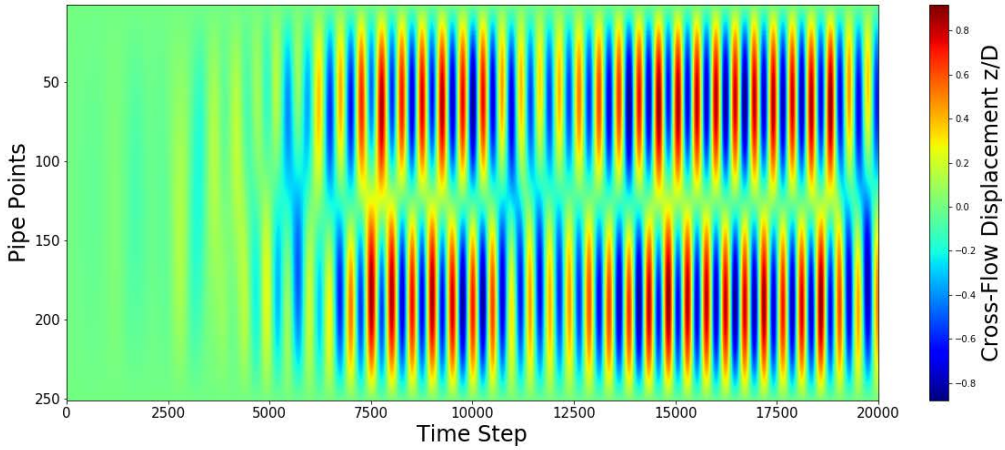

Figure 35 Cross-Flow History, Benchmark

As shown in Figure 34, maximum displacement of in-line direction occurs at the middle part of the pipe, and the amplitude of which is about 4.0 pipe diameter. For cross-flow direction, a clear vibration pattern is shown after time step 5000, and the

vibration amplitude is about 0.8 diameter. Both conclusions are in accordance with the analysis conducted for a cross-section, as described previously.

4. VIV SIMULATION OF A VERTICAL PIPE INCLUDING SOIL-STRUCTURE INTERACTIONS

Two soil-structure interaction (SSI) models characterized by two p-y curves are applied to pipe VIV simulations in this section. A simplified as well as fully nonlinear p-y curves are used to study the effect of SSI on riser-conductor system VIV response. And results are analyzed and compared with those from the benchmark case introduced in the last section.

4.1. VIV Simulation of a Vertical Pipe with Simplified SSI Model

4.1.1. Description

A simplified SSI model described by Eq. (25), same as Eq. (7), is utilized in the simulation.

$$\frac{p}{p_u} = 0.24\left(\frac{y}{y_c}\right) \tag{25}$$

Which is a "partially non-linear" SSI model, for the reason that the soil ultimate resistance, p_u, is nonlinearly varying with soil depth, while the p-y relation for each depth is simplified to linear. Soil resistance force is applied to the pipe in a partitioned coupling method, as described in section 3.

The soil properties used in this simulation is given in Table 3. It is worth noting that for this case, the depth of reduced resistance, χ_r, calculated by Eq. (3), is 2.7 m. Which is 9 times pipe diameter.

Table 3 Soil Properties, 1

Parameter	Units	Value
Soil Shear Strength, c	kPa	36
Soil Effective Unit Weight, γ	N / m^3	20000
Strain of Half Maximum Stress, ε_c	1	0.009
Empirical Constant, J	1	0.5

The pipe in the fluid domain is the same as the benchmark case with length of 144.45 m and diameter of 0.3 m. Furthermore, another half of the previous length, 72.3 m, is set to under the soil bed. Soil resistance force is applied to the pipe in the soil. And the pipe is still pinned at the top whereas set free at the bottom, which is deep into the soil. Same element length of the pipe is used in the pipe motion solver.

4.1.2. Simulation Results

4.1.2.1. Fluid Domain

The fluid domain result is similar to benchmark case. Vortex generates in the early stage of the simulation, as shown in Figure 36, then starts to detach from the pipe surface and make the pipe oscillate in the cross-flow direction, as shown in Figure 37.

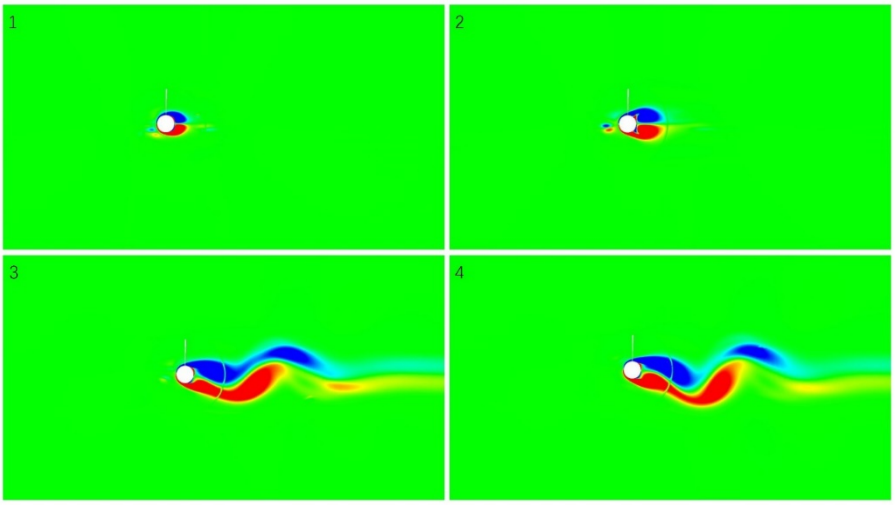

Figure 36 Vortex Generation Process, Linear SSI

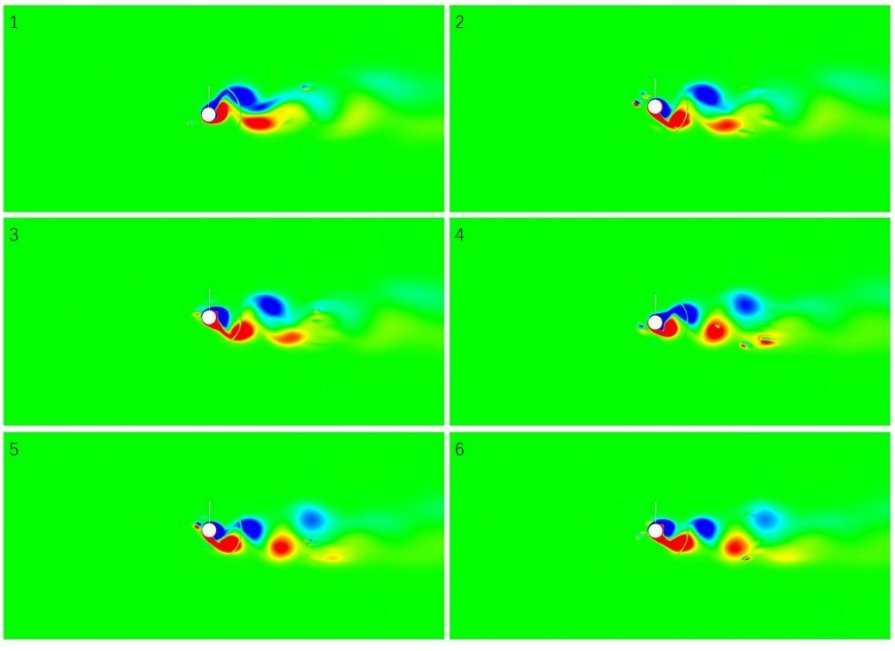

Figure 37 Vortex Shedding, Linear SSI

4.1.2.2. Pipe Motions and Comparisons

Pipe motions of selected cross-section in in-line and cross-flow directions are presented and compared with results from benchmark case in Figure 38 and Figure 39, respectively. In in-line direction, the pipe acts similarly with the benchmark case, which is the VIV simulation without SSI. The pipe deflects very fast in the initial stage, and then it reaches a nearly periodic state after time step 7500. However, the magnitude of in-line displacement is significantly reduced when SSI is take into account. An up to 40% reduction in in-line deflection is observed. The reason for this phenomenon is the soil resistance force applied to the pipe, which reduces the magnitude of pipe in-line displacement. The maximum in-line deflection of the pipe is about 2.5 times pipe diameter. For the pipe cross-flow displacement, similar conclusion can be obtained. The pipe deflects similarly with the result without SSI, whereas a reduction in the vibration magnitude is shown. The amplitude for this case is around 0.5 pipe diameter, a maximum 30% reduction in magnitude is shown when comparing with the benchmark case.

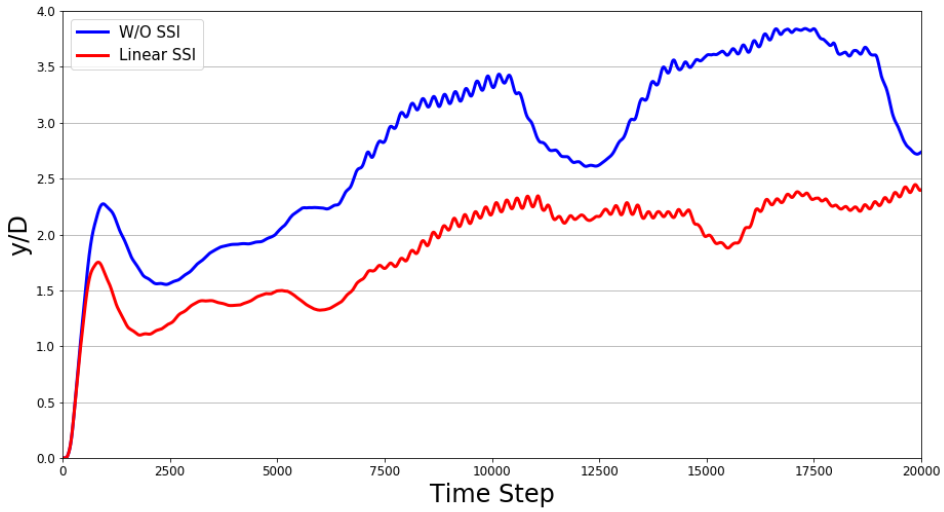

Figure 38 Comparison of Stream Wise Motions

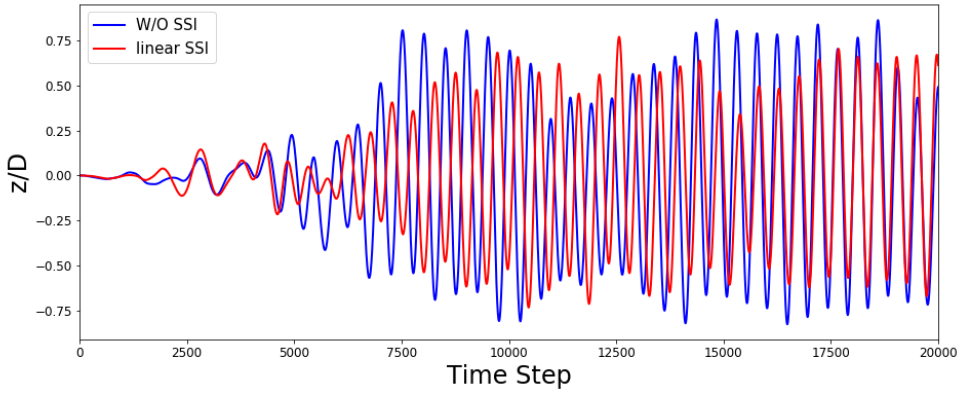

Figure 39 Comparison of Cross-Flow Motions

Pipe trajectories are plotted in Figure 40. As shown in the figure, both pipe deflect in the in-line direction and then vibrate in the cross-flow direction. However, both in-line and cross-flow displacement are reduced obviously when SSI is considered.

Trajectories from time step 17000 to 17520 are shown in particular in Figure 41 in which clear deformed “8” patterns are observed. FFT is again applied to the cross-flow response, as shown in Figure 42. The peak for this case is almost identical to the benchmark case.

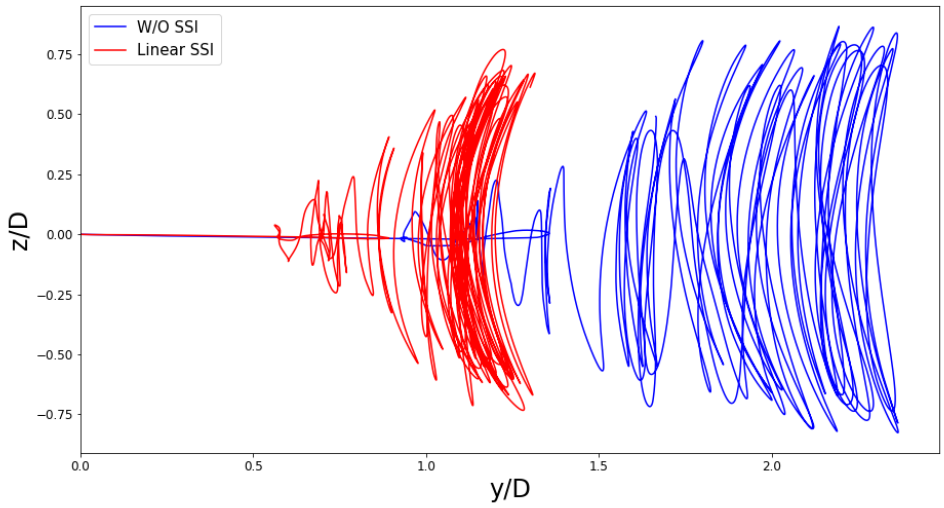

Figure 40 Comparison of Pipe Trajectories

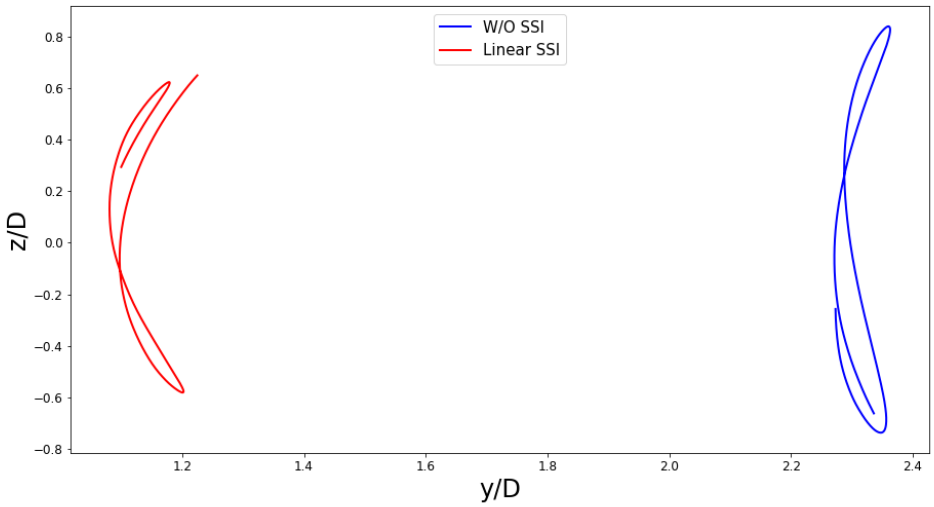

Figure 41 Comparison of Trajectories, Selected Time Steps

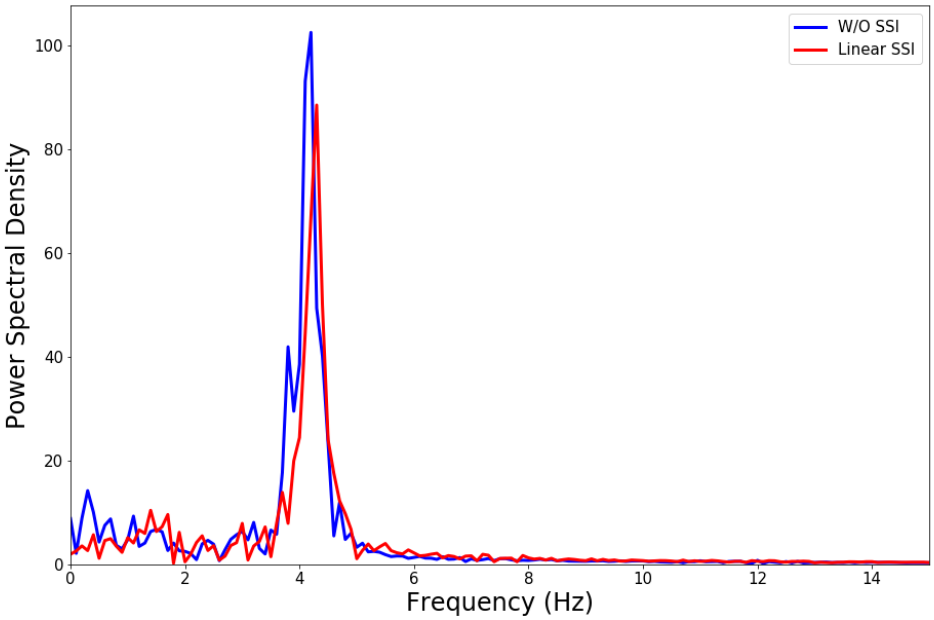

Figure 42 Comparison of Spectrums

An overview for the whole displacement with varying time steps is provided in Figure 43 and Figure 44. In the fluid domain, which is above the mudline (white line), the patterns are similar to the benchmark case. Below the mudline, displacement is very tiny comparing to the displacement in the fluid field, no significant value is shown in the two figures.

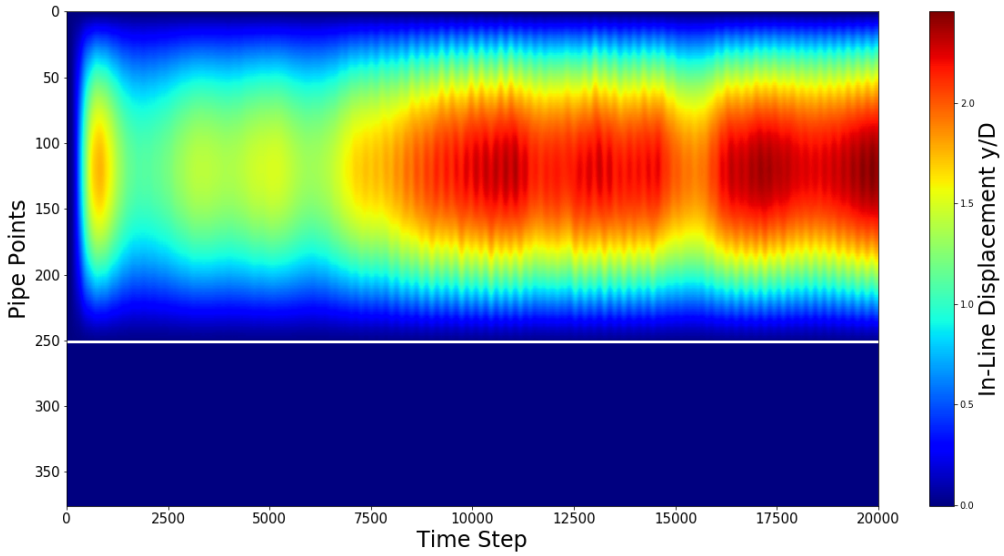

Figure 43 In-Line History, Linear SSI

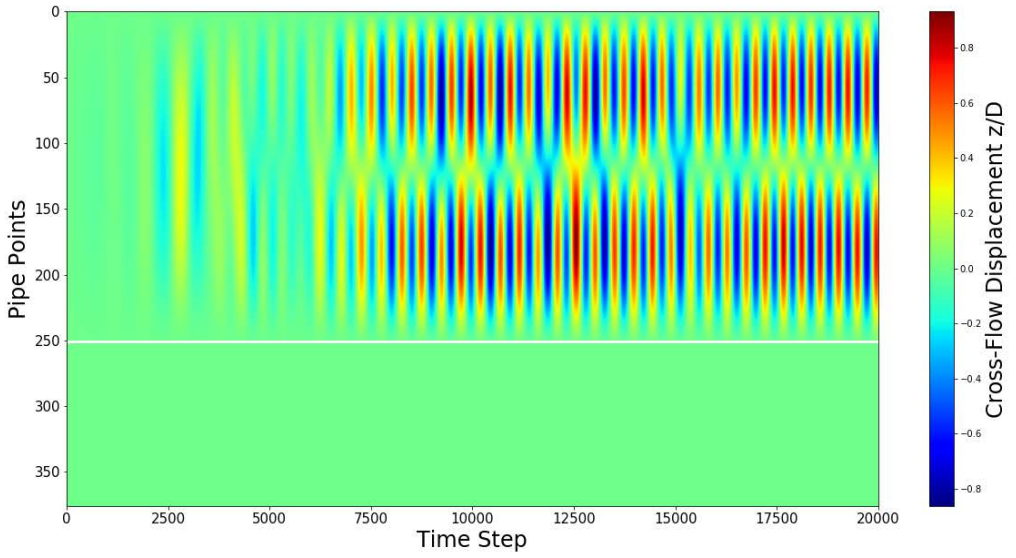

Figure 44 Cross-Flow History, Linear SSI

Comparing to the benchmark case, the pipe is not pinned at the sea bottom, that is to say, although very small, displacement at mudline exists. Displacement at mudline is of interest in this research, since in real situations, many drilling components is placed around this position. The in-line and cross-flow displacements of the pipe at mudline are given in Figure 45-48. Similar pipe response is shown at the mudline, yet the magnitude of which is much smaller comparing to that in the fluid domain. A maximum magnitude of 0.03 pipe diameter in in-line direction and 0.02 pipe diameter in cross-flow direction is obtained.

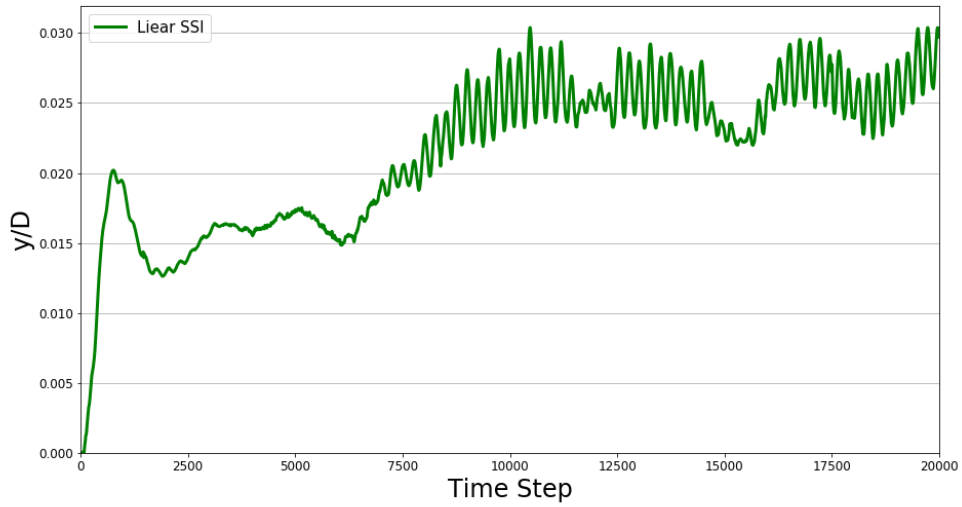

Figure 45 In-Line Motion at Mudline, Linear SSI

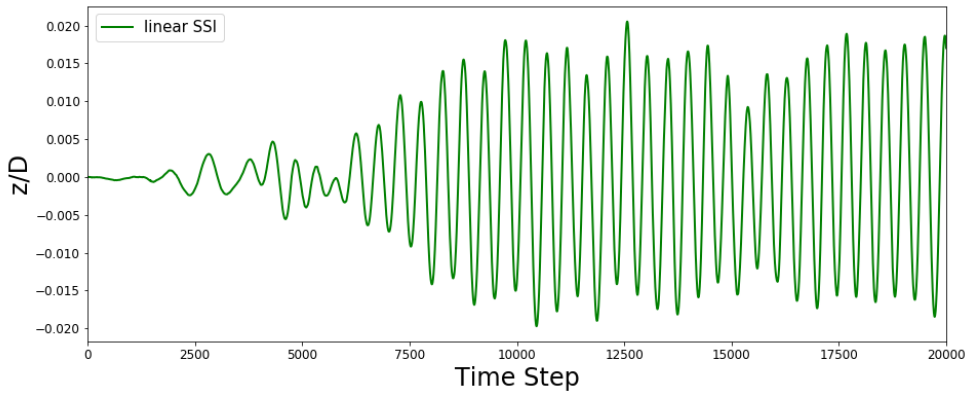

Figure 46 Cross-Flow Motion at Mudline, Linear SSI

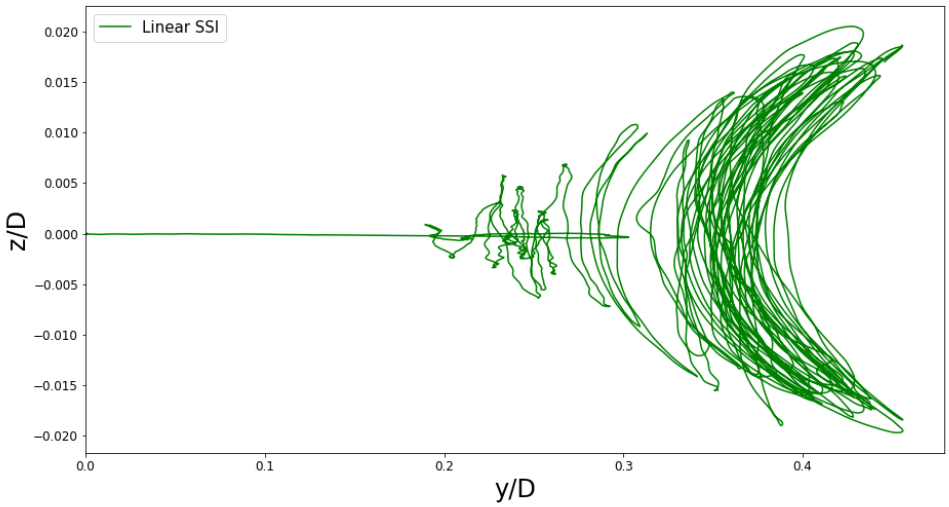

Figure 47 Trajectory at Mudline, Linear SSI

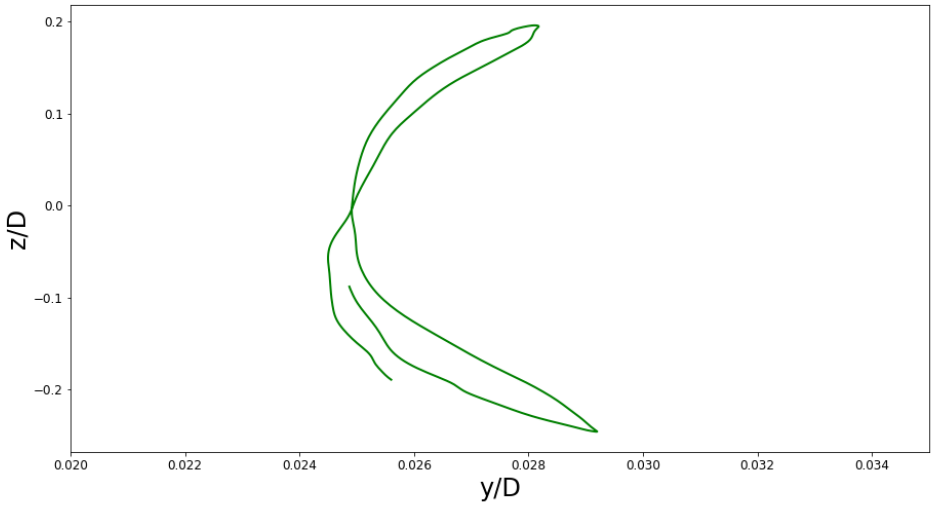

Figure 48 Trajectory at Mudline, Selected Time Steps, Linear SSI

In order to have a better illustration of the effect of SSI in pipe VIV simulations, pipe shapes at three selected time steps are presented in Figure 49 and Figure 50. When SSI is included, the pipe cross-section at mudline will experience a bending moment caused by soil resistance force, which leads to a significant reduction in pipe in-line motion, as discussed earlier. In this research, that bending moment is generated from the pipe motion (from last time step) at every time step. Which also means, comparing to simply adding a constant bending moment to the pipe end, the moment generated from SSI models will be adjusted and updated with the simulation time. When considering the cross-flow motion, the advantage of this approach is more obvious. Since when referring to the Figure 50, the direction of the bending moment will change with time, which will straightforwardly be taken into account in the pipe motion solver. Therefore, the applied SSI model ensures a more accurate bending moment for calculating the pipe displacement at each time step.

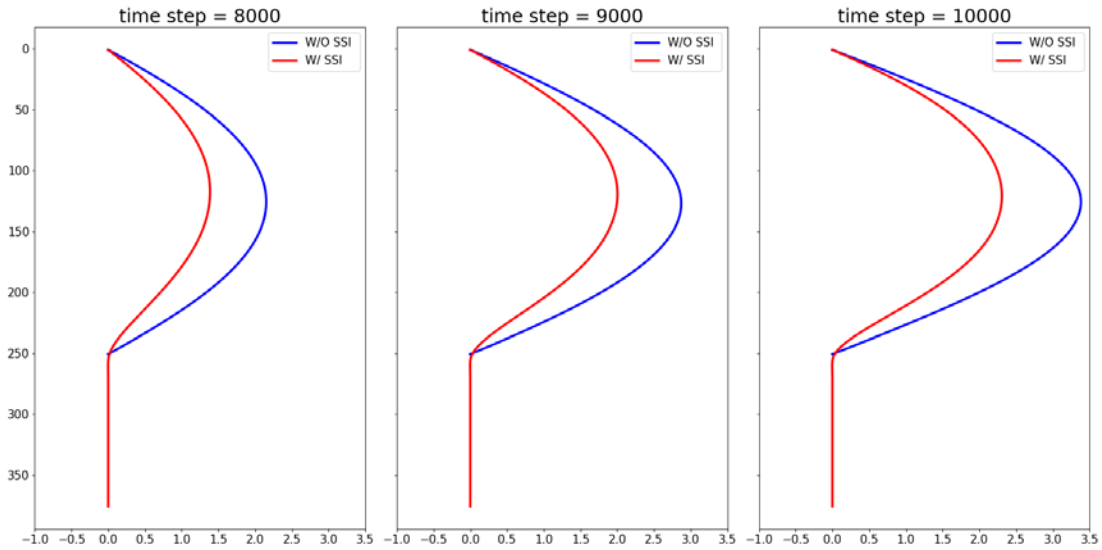

Figure 49 Pipe Shape, In-Line

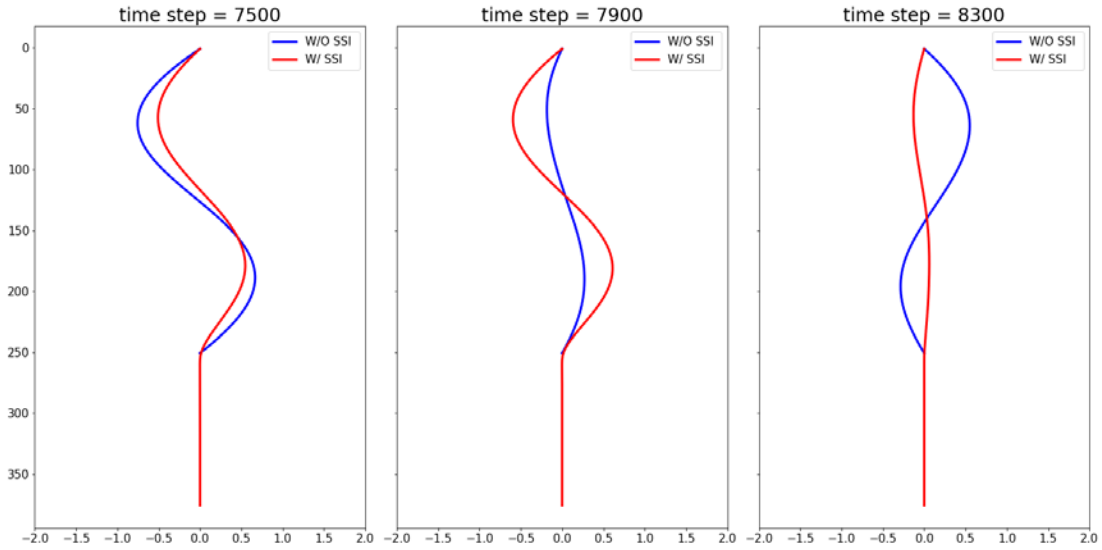

Figure 50 Pipe Shape, Cross-Flow

4.2. VIV Simulation of a Vertical Pipe with Nonlinear SSI Model

4.2.1. Description

In this section, the fully nonlinear SSI model described by the nonlinear p-y curves in Figure 17 (Eq. (5) and Eq. (6)) is applied to VIV simulations. In the axial direction (x direction in this research), the soil resistance force is nonlinear not only because of the soil ultimate resistance p_u, but also the different p-y relations for different soil depths. Moreover, the SSI model is also nonlinear in y-z plane: different p-y relations are used for lateral displacement less than $3\,y_c$, larger than $3\,y_c$ but less than $15\,y_c$, and larger than $15\,y_c$. The equations which describe this SSI model are listed as follows. It is worth mentioning that displacement "y" in these equations are absolute values. The direction of the soil resistance force is to the opposite of the pipe displacement, which will be take into consideration in the code.

At soil surface, $x = 0$:

$$\frac{p}{p_u} = 0.5\left(\frac{y}{y_c}\right)^{\frac{1}{3}} \qquad \text{for } 0 \le y \le 3y_c, \tag{26}$$

$$\frac{p}{p_u} = 0.72 - \left[0.06 - 0.06\left(\frac{x}{x_r}\right)\right]\left(\frac{y}{y_c} - 3\right) \qquad \text{for } 3y_c \le y \le 15y_c, \tag{27}$$

$$\frac{p}{p_u} = 0 \qquad \text{for } y \ge 15y_c, \tag{28}$$

For soil depth less than depth of reduced resistance, $0 \le x \le x_r$:

$$\frac{p}{p_u} = 0.5\left(\frac{y}{y_c}\right)^{\frac{1}{3}} \qquad \text{for } 0 \le y \le 3y_c, \tag{29}$$

$$\frac{p}{p_u} = 0.72 - \left[0.06\left(\frac{y}{y_c} - 3\right)\right] \qquad \text{for } 3y_c \le y \le 15y_c, \tag{30}$$

$$\frac{p}{p_u} = 0.72\left(\frac{x}{x_r}\right) \qquad \text{for } y \ge 15y_c, \tag{31}$$

For soil depth larger than depth of reduced resistance, $x > x_r$:

$$\frac{p}{p_u} = 0.5\left(\frac{y}{y_c}\right)^{\frac{1}{3}} \qquad \text{for } 0 \le y \le 3y_c, \tag{32}$$

$$\frac{p}{p_u} = 0.72\left(\frac{x}{x_r}\right) \qquad \text{for } y \ge 3y_c. \tag{33}$$

Soil Properties and pipe parameters are the same as the last case, as listed in Table 4.

Table 4 Soil Properties, 2

Parameter	**Units**	**Value**
Pipe Diameter	m	0.3
Pipe length in Fluid Domain	m	144.45
Pipe length in Soil	m	72.23
Bending Stiffness	$N \cdot m^2$	6.85E6
Top Pretension	N	1.84E5
Soil Shear Strength, c	kPa	36
Soil Effective Unit Weight, γ	N / m^3	20000
Strain of Half Maximum Stress, ε_c	1	0.009

Table 4 Continued

Empirical Constant, J	1	0.5
Depth of Reduced Resistance, χ_r	m	2.7

4.2.2. Simulation Results

4.2.2.1. Fluid Domain

The fluid domain view for this case is similar to the previous two cases, benchmark case and the case with linear SSI. The pipe deflects in the in-line direction and vortex starts to generate at the beginning of the simulation, as shown in Figure 51. And then, approximately starting from time step 3000, the vortex starts to shed from the pipe surface, making the pipe oscillate in the cross-flow direction, as shown in Figure 52.

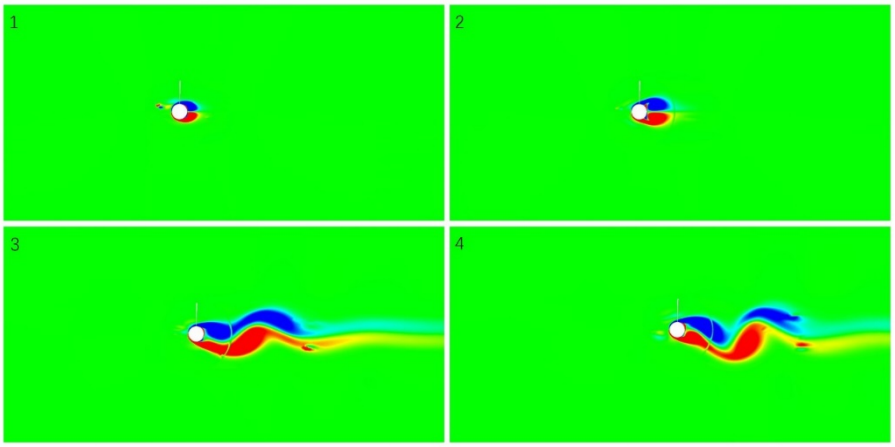

Figure 51 Vortex Generation Process, Nonlinear SSI

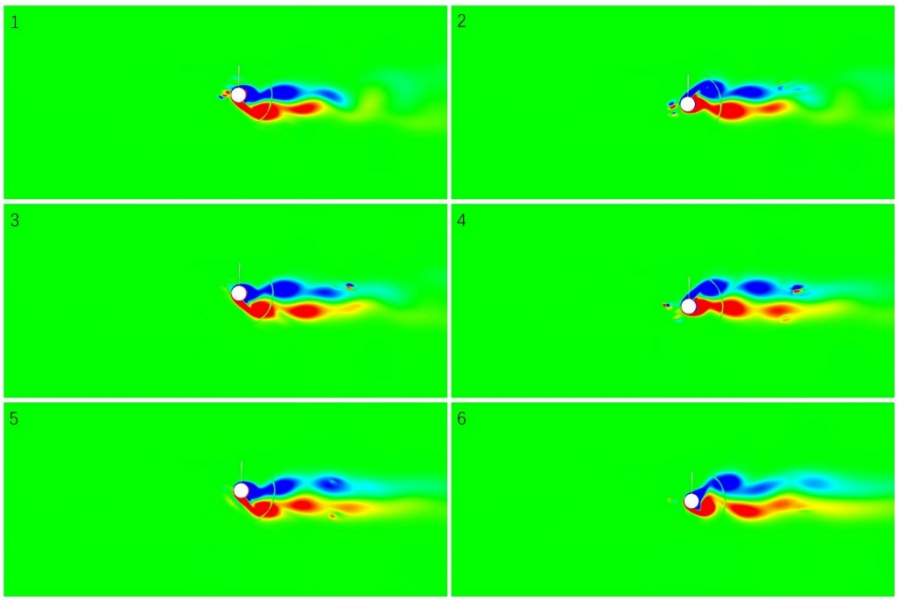

Figure 52 Vortex Shedding, Nonlinear SSI

4.2.2.2. Pipe Motions and Comparisons

Pipe motions in in-line and cross-flow directions are plotted and compared with those of obtained from former two cases in Figure 53 and Figure 54, respectively. For in-line motion, the behavior of the pipe obtained in this case to which a nonlinear SSI model is applied, is similar with the case with the linear SSI model. A significant reduction of about 40% in maximum magnitude of in-line displacement is also observed in this case. In the two cases to which SSI models are applied, pipe in-line motions are almost identical until they reach the first peak at time step around 1000. And then after time step 2500, two curves start to look differently due to the different SSI models. For linear SSI model, soil resistance increases linearly with increasing pipe displacement. To the contrary, for nonlinear SSI model, soil resistance will reach a maximum value beyond which soil resistance will remain constant, which means different equivalent

moment from the soil will be applied to the pipe in the fluid domain as the time step increases. Moreover, modification for p-y curve at soil surface is specially made to account for the weak soil resistance at that depth. However, the difference in pipe in-line motion between these two cases is not significant, and the maximum displacements for both cases are about 2.5 times pipe diameters.

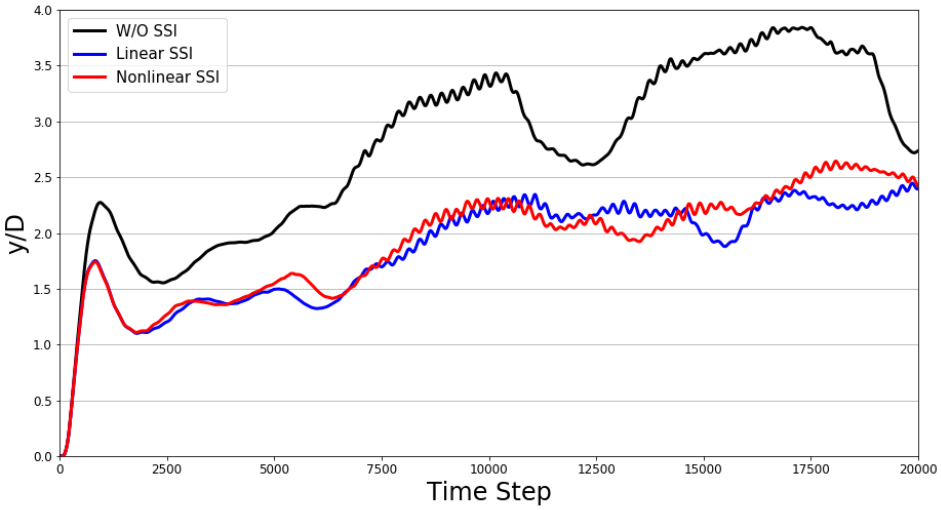

Figure 53 Pipe Stream Wise Motions

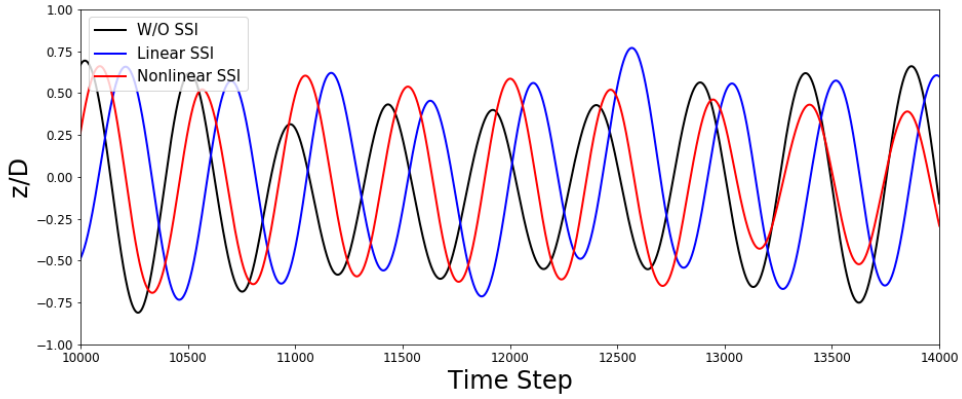

Figure 54 Pipe Cross-Flow Motions, Selected Time Steps

Pipe trajectories for all three cases are given in Figure 55. From the figure, one can tell that results obtained from simulations with two SSI models are similar, only a slight difference exists between those two. Detailed trajectories from time step 17000 to 17520 are provided in Figure 56 in which clear deformed “8” patterns are again shown. FFT results for cases with SSI models are shown in Figure 57, in which two peaks are almost identical.

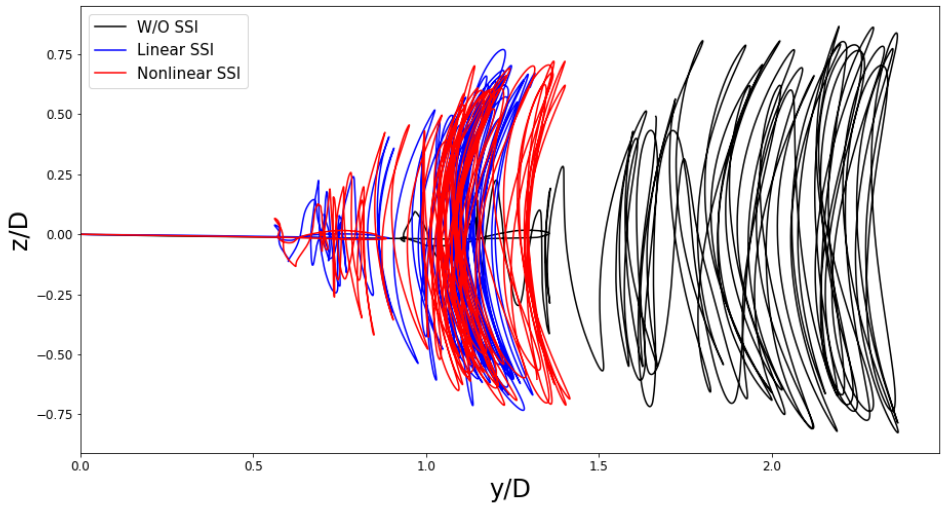

Figure 55 Pipe Trajectories

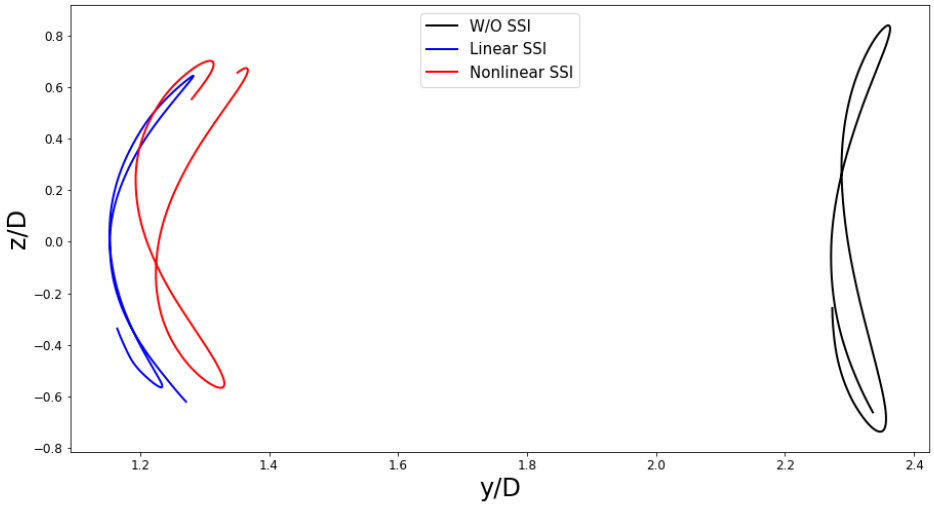

Figure 56 Trajectories, Selected Time Steps

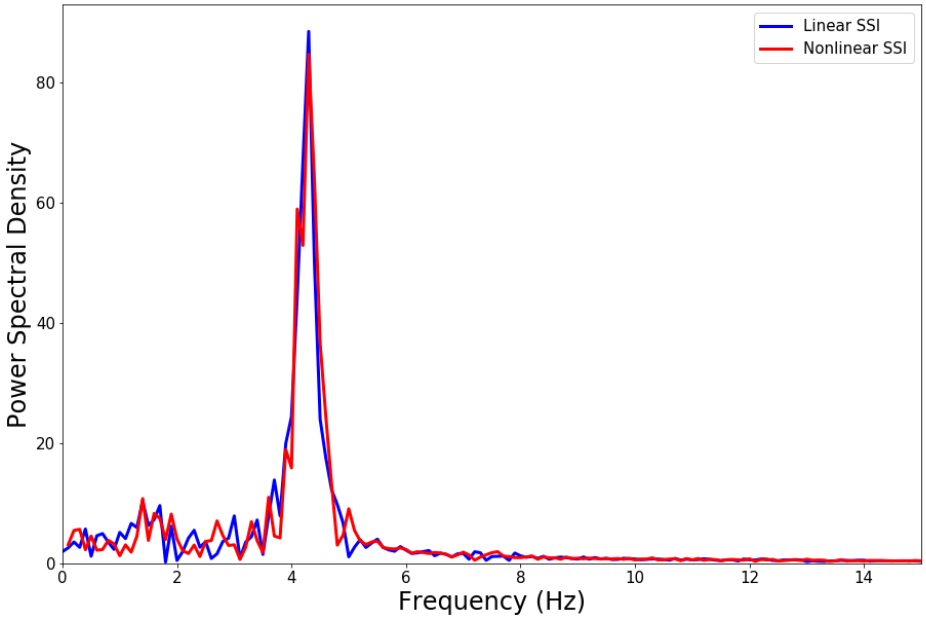

Figure 57 Spectrums

Overviews for all pipe nodes in in-line and cross-flow directions are once again provided in Figure 58 and Figure 59, respectively. Comparing to Figure 43 and Figure 44, which are the plots for linear SSI case, no significant difference is observed, and this is in accordance with former discussions.

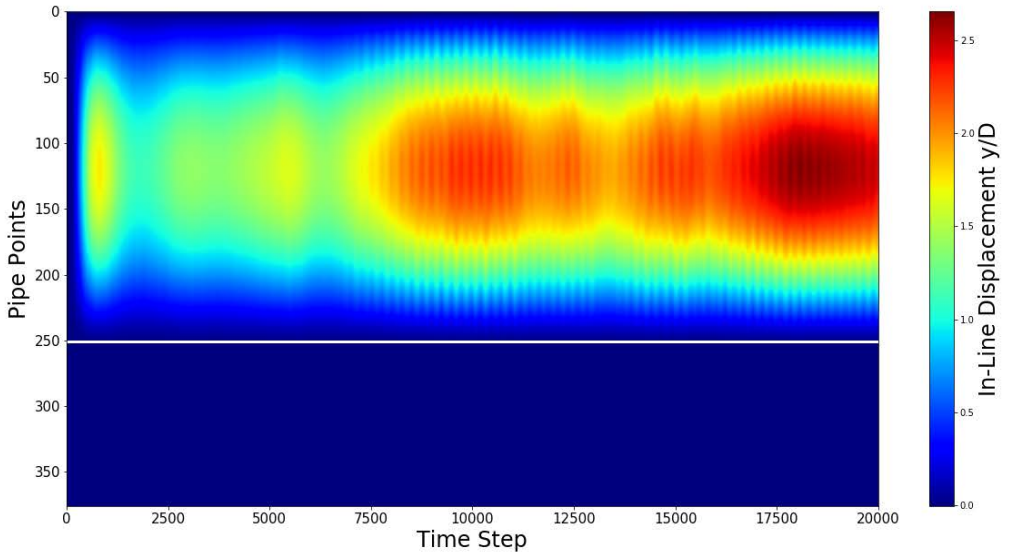

Figure 58 In-Line History, Nonlinear SSI

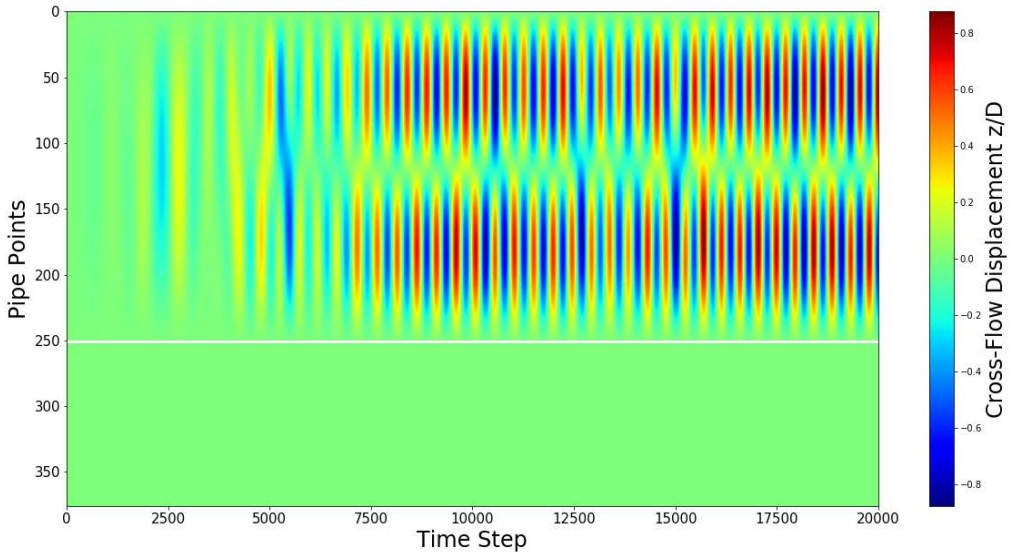

Figure 59 Cross-Flow History, Nonlinear SSI

Pipe motions at mudline are compared in Figure 60-63. As shown in pipe in-line and cross-line motions, a nonnegligible difference of magnitude is shown. Comparing to the linear SSI model, result from Nonlinear SSI model is smaller. That is expected and the reason can be explained by Eq. (26). For both two cases, the lateral displacements are smaller than y_c, which is in the range of 0 to y_c, therefore, much larger soil resistance force will be applied to the pipe comparing to the non-linear model described by Eq. (26). That means smaller displacement will be obtained from the nonlinear SSI model case. A more obvious look is shown in the trajectory plot. The pipe trajectory from nonlinear SSI model is on the left, while the trajectory from the linear SSI model is on the right. Detailed trajectories are also provided in the next figure.

Figure 60 In-Line Motions at Mudline, Nonlinear SSI

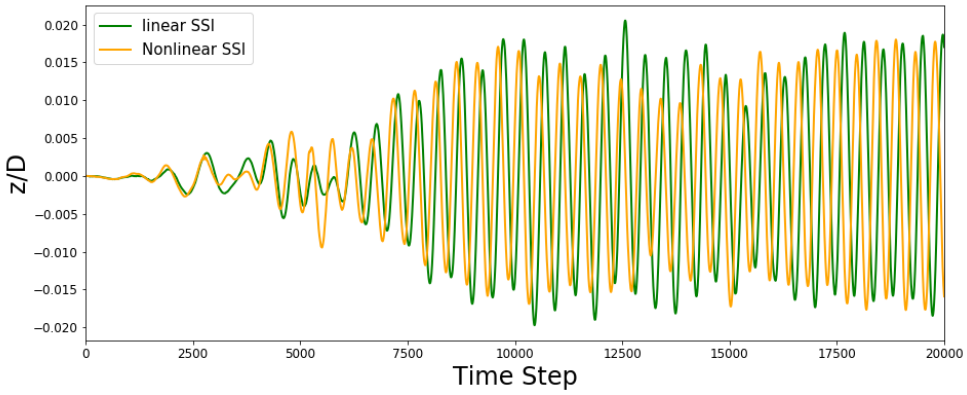

Figure 61 Cross-Flow Motions at Mudline, Nonlinear SSI

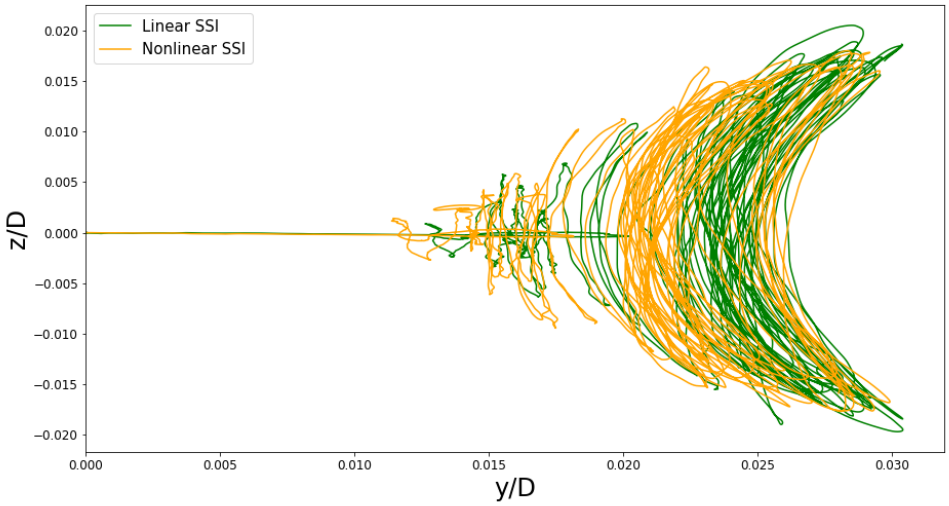

Figure 62 Trajectories at Mudline, Nonlinear SSI

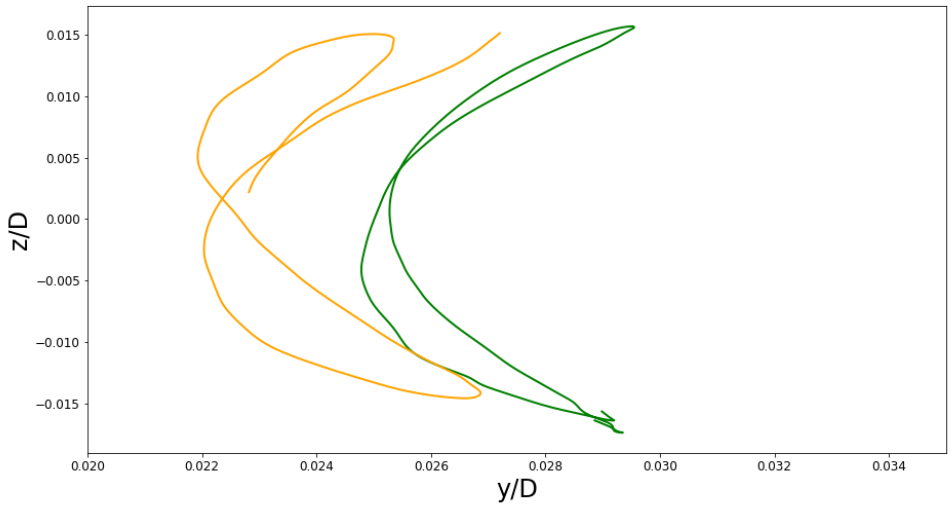

Figure 63 Trajectory at Mudline, Selected Time Steps, Nonlinear SSI

4.3. Summary

Two SSI models, linear and nonlinear models, are applied to the pipe VIV simulations to account for the soil resistance force. Significant reduction of pipe responses in both in-line and cross-flow directions is observed. Pipe motions calculated by those two models are not significantly different in the fluid domain, however, at the soil surface, noteworthy pipe motion difference is shown: smaller displacement both in in-line and cross-flow direction is obtained due to lager soil resistance force described by the nonlinear SSI model when displacement is less than y_c. Therefore, soil-structure interaction is a crucial part in VIV simulations of riser-conductor system and should not be ignored.

5. EFFECTS OF SOIL PROPERTIES ON RISER-CONDUCTOR VIV SIMULATIONS

Soil strength c and soil effective unit weight γ are two key parameters that characterize soil properties, and thus further clarification is required for analysis. In former discussions, soil strength and the effective unit weight of soil were arbitrarily set to 36 kPa and 20000 N/m^3, respectively, according to the most commonly used values. However, in reality, those two soil properties should be directly obtained from laboratory tests for soil in specific locations where drilling will be operated. Both the soil strength and the soil effective unit weight will affect the soil ultimate resistance p_u as well as the depth of reduced resistance x_r, as described in Eq. (1) and Eq. (3), thus different soil resistance force will be applied to the riser-conductor system.

Therefore, in this section, the effects of the two aforementioned soil properties on the VIV simulations are studied, and pipe motions at mudline are compared and analyzed. Note that for discussions in this section, the nonlinear SSI model is adopted.

5.1. Effect of Soil Strength

First, pipe VIV simulation with soil strength c of 12 kPa, 24 kPa and 36 kPa are conducted, with a same soil effective weight of 20000 N/m^3. Note that the depth of reduced soil resistance x_r will also vary with different values of c.

Pipe motion histories of both in-line and cross-flow (stead state) directions are given in Figure 64 and Figure 65, respectively. And as shown in Figure 66, trajectory from soil strength of 36 kPa is on the left of the figure, while trajectory from soil strength of 12 kPa is on the right. It can be concluded that with decreasing soil strength, pipe motions in both in-line and cross-flow directions increases. That is reasonable since larger soil strength results to larger soil resistance force, as described in Eq. (1) and Eq. (2), which will confine the pipe trajectory to a smaller area.

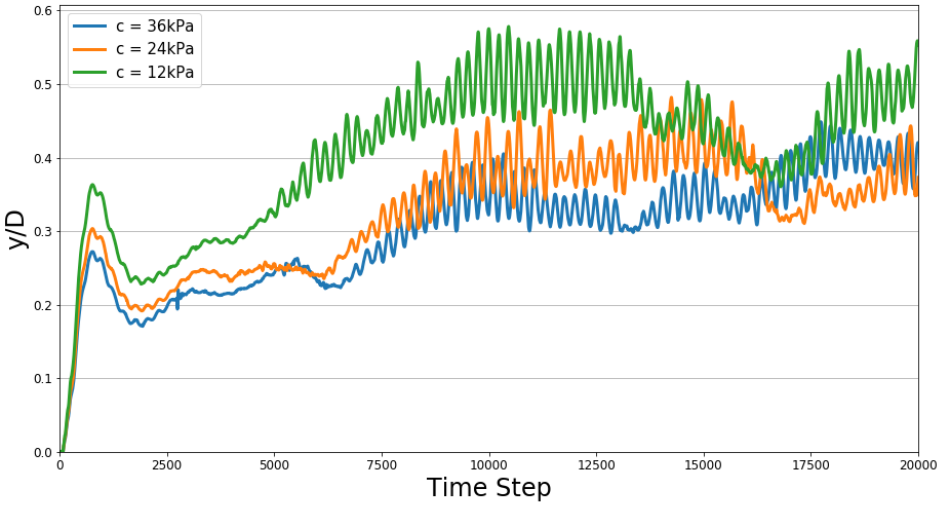

Figure 64 In-Line Motions at Mudline for Different Soil Strength

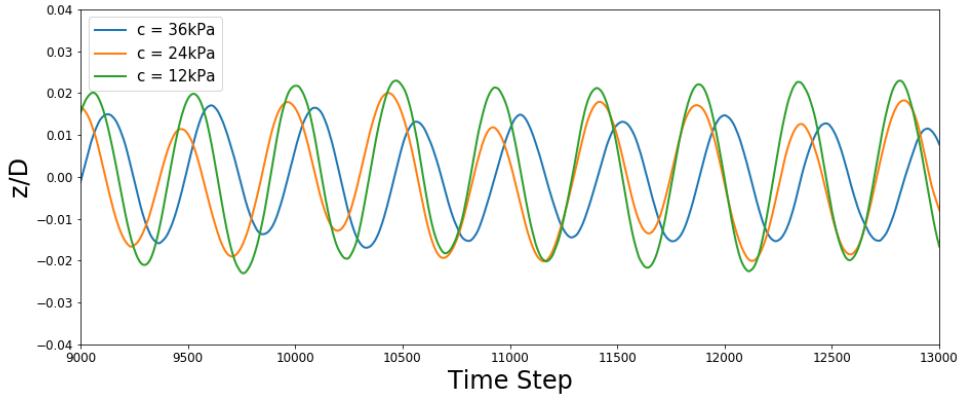

Figure 65 Cross-Flow Motions at Mudline for Different Soil Strength, Time Step 9000 to 13000

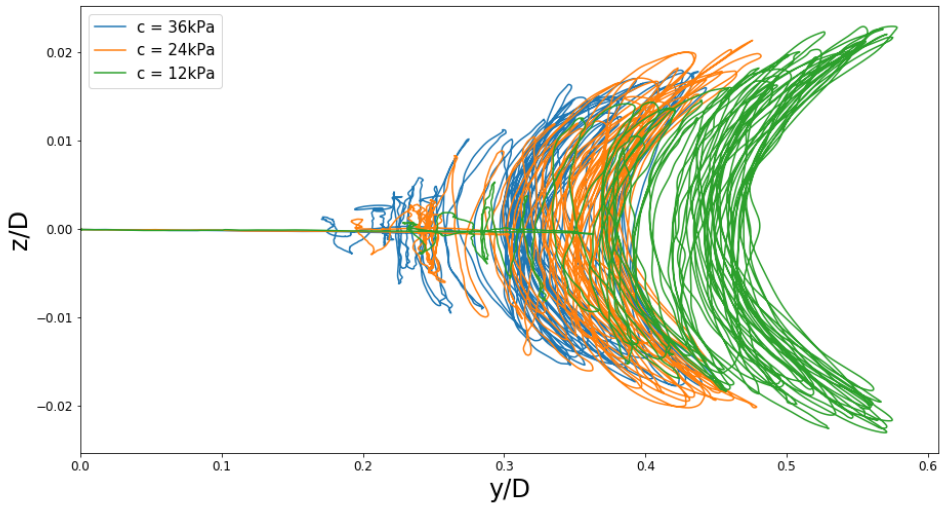

Figure 66 Trajectories at Mudline for Different Soil Strength

The maximum displacement in in-line and cross-flow directions obtained from those three cases are shown in Figure 67. Apparently, the maximum displacement

reduces with the increasing soil shear strength. That is to say, for “soft soil”, pipe motion at mudline will be more significant.

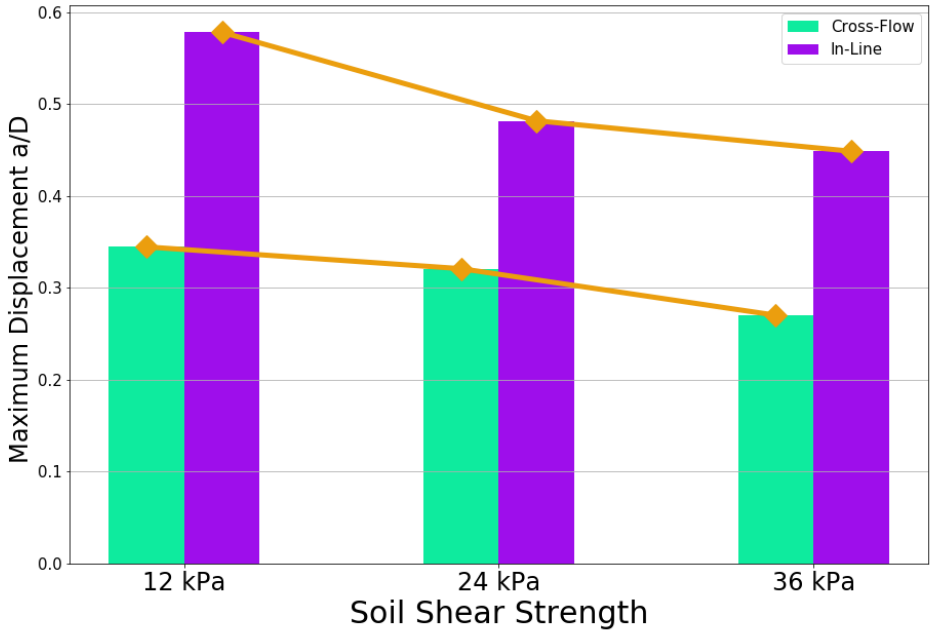

Figure 67 Maximum Displacements with Varying Soil Strength

5.2. Effect of Soil Effective Unit Weight

Different soil effective unit weight is then applied to the nonlinear SSI model. The unit weight of soil γ is a parameter associated with the void ratio of the soil e, and is defined as,

$$\gamma = \frac{\gamma_w \left(G_s + e\right)}{1+e} \tag{34}$$

In which γ_w is the unit weight of water, G_s is the specific gravity of soil. And a larger value of γ means a larger value of soil void ratio. The value of γ could also vary with the soil depth. However, in this research, the change of γ with soil depth is not considered. Instead, in this section, three different values of γ, 15000 N/m^3, 20000 N/m^3 and 25000 N/m^3 with a same value of soil strength (12 kPa), are applied to the VIV simulations. Note that the depth of reduced soil resistance χ_r will also vary with different values of γ.

Pipe motions in in-line and cross-flow directions and the pipe trajectories are shown in Figures 68-70. Comparing to Figures 64-66, no remarkable difference is shown, since the curves are overlapping each other. The maximum displacement in in-line and cross-flow directions with varying γ is also provided, as shown in Figure 71. For cross-flow direction, tiny increases are observed while the value of γ is increasing. However, for in-line direction, the maximum displacement is increased while γ increases to 20000 N/m^3 from 15000 N/m^3, and reduced while γ increases to 25000 N/m^3 from 20000 N/m^3. Therefore, the value of soil effective unit weight γ may not have a significant effect on the simulation as soil shear strength do.

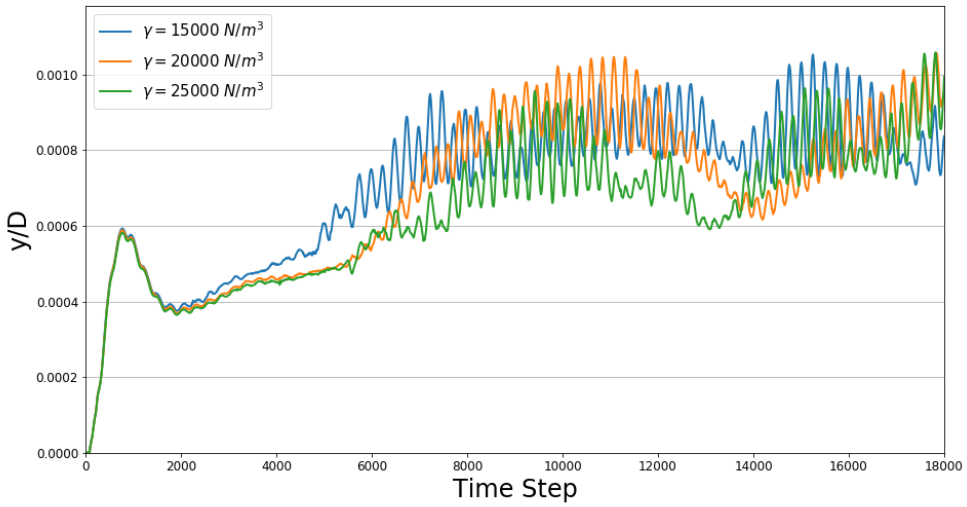

Figure 68 In-Line Motions at Mudline for Different Soil Unit Weight

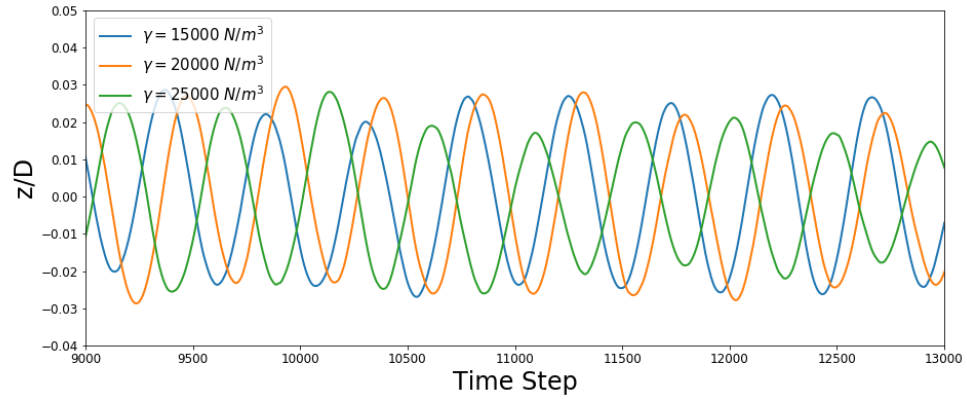

Figure 69 Cross-Flow Motions at Mudline for Different Soil Unit Weight, Time Step 9000 to 13000

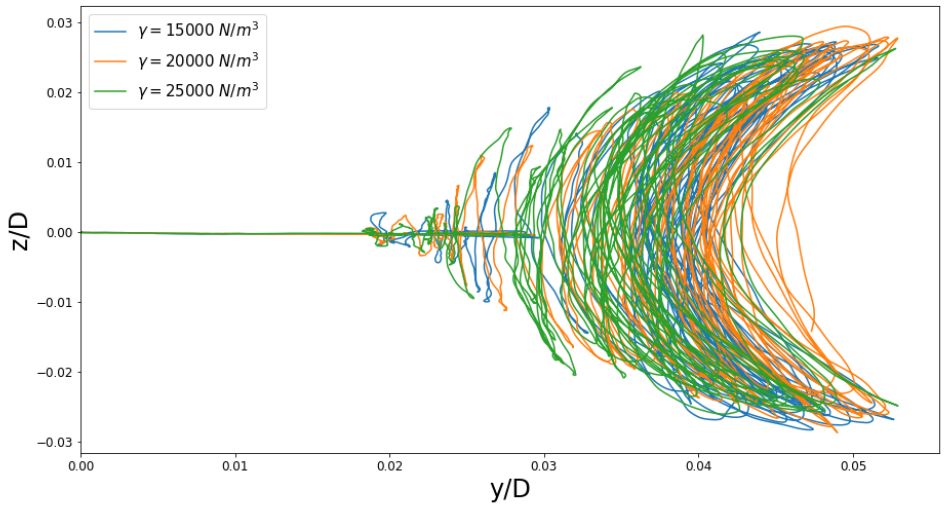

Figure 70 Trajectories at Mudline for Different Soil Unit Weight

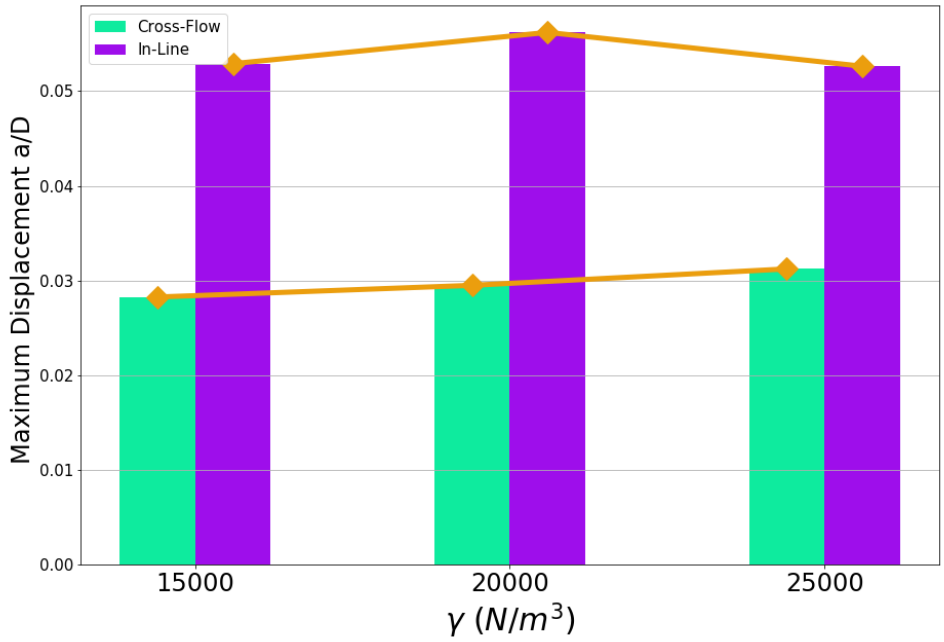

Figure 71 Maximum Displacements with Varying Soil Effective Unit Weight

5.3. Summary

The effects of two key soil properties on riser-conductor system VIV simulations are discussed in this section, which are soil shear strength c and soil effective unit weight γ. And pipe motion at mudline is presented and analyzed. When the soil shear strength increases, the magnitude of pipe displacement in both in-line and cross-flow directions are reduced. However, for soil effective unit weight, with the value of γ increasing, no significant change in displacement magnitude is shown.

6. SUMMARY AND CONCLUSIONS

6.1. Summary

Deepwater drilling riser-conductor systems are susceptible to VIV. Previous researchers have rarely take Soil-Structure Interactions into account when study on the VIV response of riser-conductor systems, and experiment data is especially absent. In this research, a numerical approach for riser-conductor VIV analysis is developed based on pipe VIV simulations conducted by Prof. Chen and his former students. The method is realized by coupling the fluid domain solver, Finite-Analytic Navier-Stokes (FANS) code, and the pipe motion solver to which the SSI models are added. The SSI is reached by modeling the soil resistance force according to a published p-y curve which specifies the relation between pipe lateral displacement and soil resistance force.

First, the riser-conductor system is modeled as a distributed tension beam, and the soil model is validated by a case in which static force is applied. The result obtained from our method shows a very good agreement with the results from FEA and other published analytical solutions.

Second, a riser VIV simulation without considering SSI is conducted to serve as a benchmark case for following simulations in which SSI models are applied. And then, two SSI models are adopted in the VIV simulations of riser-conductor systems. A simplified SSI model (referred to as linear) is firstly used in the simulation, in which lateral soil resistance is linearly varying with lateral displacement while ultimate soil resistance varies with the soil depth nonlinearly. A significant reduction, 20% to 40% in

magnitude, in both pipe in-line and cross-flow directions comparing to the benchmark case are observed. And pipe motion at mudline is also obtained instead of zero displacement in benchmark case. Following the simplified SSI model, the fully nonlinear SSI model (referred to as nonlinear) is applied to the VIV simulation of riser-conductor simulation. The result is similar to the linear SSI model case in magnitude since the maximum amplitude is not very large for both cases. To conclude, SSI model is crucial to the simulations of riser-conductor systems. Meanwhile, simplified SSI model is also applicable in small amplitude VIV simulations.

Finally, the effect of two key soil properties, soil shear strength and soil effective unit weight, on the pipe VIV simulations are analyzed. It is shown that with both soil shear strength and soil effective unit weight decreasing, the displacement of the system at mudline is amplified.

In conclusion, a fully three dimensional CFD approach for analyzing the VIV of deepwater drilling and production riser-conductor systems is provided. This research contributes knowledge and insight to future design and analysis of riser-conductor systems

6.2. Recommendations for Future Research

Recommendations for future study include the following:

1) Experiments of riser VIV including Soil-Structure Interactions needs to be carried out to further validate the numerical methods. SSI is extremely complicated because of the nonlinearity of the soil. Certain modifications may be required to better model the

soil resistance force.

2) The nonlinear p-y curves adopted in this research is suggested by Matlock (1970), as mentioned before. However, the points in the p-y curves which characterize the SSI are “basically empirical”. Since the curves generated are required to fit the field test data. Therefore, specific p-y curves should be generated for specific soil specimen, otherwise large errors may occur.

3) Soil is likely to be liquefied under cyclic lateral loads. If liquefaction occurs, soil shear strength will be lost, and soil resistance force will be reduced severely, thus large lateral displacement at mudline of riser-conductor system might be induced. Therefore, research to analyze the soil behavior under pipe cyclic motions should be conducted.

REFERENCES

Ai, S., & Sun, L. (2010). Vortex induced vibration response of a rigid cylinder supported with perfectly plastic nonlinear springs. Journal of Vibration and Shock, 29(11), 21-25.

American Petroleum Institute. (2010). API Recommended Practice 2A-WSD.

Basu, D., & Salgado, R. (2007). Elastic analysis of laterally loaded pile in multi-layered soil. Geomechanics & Geoengineering, 2(3), 183-196.

Chen, H.C., Chen, C. R., Huang, K. (2013). CFD Simulation of Vortex-Induced and Wake-Induced Vibrations of Dual Vertical Risers, Proceedings of the Twenty-third (2013) International Offshore and Polar Engineering Anchorage, July, 2013, Alaska, USA.

Chen, H. C., Patel, V. C., & Ju, S. (1990). Solutions of Reynolds-Averaged Navier-Stokes equations for three-dimensional incompressible flows. Journal of Computational Physics, 88(2), 305-336.

Choi, Y. S., Basu, D., Salgado, R., & Prezzi, M. (2014). Response of Laterally Loaded Rectangular and Circular Piles in Soils with Properties Varying with Depth. Journal of Geotechnical & Geoenvironmental Engineering, 140(4), 04013049.

El Naggar, M. H., & Novak, M. (1995). Nonlinear lateral interaction in pile dynamics. Soil Dynamics and Earthquake Engineering, 14(2), 141–157.

Gazetas, G., & Dorbry, R. (1984). Horizontal response of piles in layered soils. Journal of Geotechnical Engineering, 110(1), 20-40.

Han, F., Salgado, R., & Prezzi, M. (2015). Nonlinear analyses of laterally loaded piles – a semi-analytical approach. Computers & Geotechnics, 70, 116-129.

Huang, K., Chen, H. C., Chen, C. R. (2007). Riser VIV analysis by a CFD approach, in: Proceedings of the 17th International Offshore and Polar Engineering (ISOPE) Conference, July 2007, Lisbon, Portugal.

Huang, K., Chen, H. C., & Chen, C. R. (2011). Numerical Scheme for Riser Motion Calculation During 3-D VIV Simulation. Journal of Fluids & Structures, 27(7), 947-961.

Liang, A., Wang, S., Li, L., Liu, X., Wang, Z., & Wen, X. (2014). Study on influence of soil-pile nonlinear interaction on vehicle-bridge coupling vibration. Engineering Mechanics.

Matlock, H. (1970). Correlation for Design of Laterally Loaded Piles in Soft Clay. Offshore Technology in Civil Engineering (Vol.1, pp.77-94). ASCE.

Matlock, H., & Reese, L. C. (1960). Generalized solutions for laterally loaded piles. Geotechnical Special Publication, 127(118), 1220-1248.

Nogami, T., & Konagai, K. (1988). Time Domain Flexural Response of Dynamically Loaded Single Piles. Journal of Engineering Mechanics, 114(9), 1512–1525.

Nogami, Toyoaki; Konagai, Kazuo; and Otani, Jun (1991). Nonlinear Time Domain Numerical Model for Pile Group Under Transient Dynamic Forces. International Conferences on Recent Advances in Geotechnical Earthquake Engineering and Soil Dynamics, 25.

Novak, M., & Works, V. I. (1974). Dynamic stiffness and damping of piles. Canadian Geotechnical Journal, 11(4), 574–598.

Olusola Ayandire Ilupeju (2014). Soil-Spring Model for Fatigue Evaluation of Cyclic-Loaded Offshore Conductors. Master of Science Thesis, Texas A&M University.

Pontaza, J.P., Chen, C.R. and Chen, H.C. (2004). Chimera Reynolds averaged Navier-Stokes simulations of vortex-induced vibration of circular cylinders. Proceedings of the International ASCE Conference: Civil Engineering in the Oceans VI, pp 166-176.

Pontaza, J.P. and Menon, R.G. (2009). Prediction of VIV Response of a Flexible Pipe by Coupling a Viscous Flow Solver and a Beam Finite Element Solver. PaperOMAE2009-79150, 28th Intl Conference on Ocean, Offshore and Artic Engineering, Honolulu, Hawaii.

Reese, L. C. (1974). Analysis of Laterally Loaded Piles in Sand. Offshore Technical Conference, Texas (pp.95-105).

Tognarelli, M. A., Taggart, S., & Campbell, M. (2008). Actual VIV fatigue response of full scale drilling risers: with and without suppression devices. In ASME 2008 27th International Conference on Offshore Mechanics and Arctic Engineering (pp. 513-525). American Society of Mechanical Engineers.

Trim, A. D., Braaten, H., Lie, H., and Tognarelli, M. A. (2005). Experimental Investigation of Vortex-Induced Vibration of Long Marine Risers. J. Fluids Struct., 21, pp. 335–361.

Wilde J. J. & Huijsmans, R. H. (2004). Laboratory investigation of long riser VIV response. In the Fourteenth International Offshore and Polar Engineering Conference. International Society of Offshore and Polar Engineers.

Xiao, F. (2015). CFD Simulation of Vortex-Induced Vibrations of Free Span Pipelines Including Pipe-Soil Interactions. Master's thesis, Texas A & M University.

Yao, W., Huai-Rui, W., Cheng, Z., & Wu, Y. (2011). Nonlinear numerical analysis of super-long piles based on p-y curves. Chinese Journal of Geotechnical Engineering, 33(11), 1683-1690.

Zhu, Y. (2017). Numerical Simulation of Vortex-Induced Vibrations of Free Span Pipelines Including Nonlinear Soil Models. Master's thesis, Texas A & M University.